AB INITIO COMPUTATIONAL STUDY OF ELECTRONIC STRUCTURE AND EFFECT OF APPLIED PRESSURE ON SUPERCONDUCTING PROPERTIES OF NB_3SN AND TI; NB_3SN

NYANDIKA A. NYANGARISA

A Thesis Submitted to the Institute of Postgraduate Studies of Kabarak University in Partial Fulfilment of the Requirements for the Award of the Master of Science in Physics Degree

KABARAK UNIVERSITY

NOVEMBER, 2025

DECLARATION

1. I do declare that:

   i. This thesis is my own original work, and to the best of my knowledge, it has not been presented for the award of a degree in any university or college.

   ii. That the work has not incorporated material from other works or a paraphrase of such material without due and appropriate acknowledgement.

   iii. That the work has been subjected to processes of anti-plagiarism and has met Kabarak University's 15% similarity index threshold.

2. I do understand that issues of academic integrity are paramount, and therefore, I may be suspended or expelled from the University, or my degree may be recalled for academic dishonesty or any other related academic malpractices.

Signed:_____ Date:_____

Nyandika A. Nyangarisa

GMP/M/0679/05/22

RECOMMENDATION

To the Institute of Postgraduate Studies:

The thesis entitled "**AB INITIO Computational Study of Electronic Structure and Effect of Applied Pressure on Superconducting Properties of NB_3SN AND TI; NB_3SN** written by **Nyandika A. Nyangarisa**, is presented to the Institute of Postgraduate Studies of Kabarak University. We have reviewed the thesis and recommend it be accepted in partial fulfilment of the requirement for the award of the Master of Science in Physics Degree.

Signed:_____ Date:_____

Dr. Phillip Otieno Nyawere

Department of Physical and Biological Sciences

Kabarak University

Signed:_____ Date:_____

Dr. Kebenei Sella J.

Department of Physical and Biological Sciences

Kabarak University

COPYRIGHT

ACKNOWLEDGEMENT

I first and foremost acknowledge the Lord Jesus Christ, my saviour, for His providence and protection. It has been by His grace.

I appreciate my supervisors, Dr. Phillip Otieno Nyawere and Dr. Sella J. Kebenei, for their encouragement, tireless work, and their time involved in doing this work. I highly appreciate the entire Kabarak University, especially the Kabarak University Online, for the assistance they provided me throughout my studies.

My gratitude goes to my family: parents, Mr. Evans Nyandika and Mrs. Debora Magoma, my brother, and my sisters for their prayers, financial and moral support. Thanks to the ICT personnel, especially Mr. Reuben Sirma, who constantly assisted me with network and computer challenges.

I sincerely appreciate the Quantum Espresso developers for their work in preparing the Quantum ESPRESSO code used in all calculations in this work. I would like to express my gratitude to the National Council of Science and Technology-Kenya for permitting me to conduct my research and for providing the research grant. I thank the Centre for High Performance Computing (CHPC), Cape Town (South Africa), for providing an HPC facility used in all calculations in this thesis. I also extend my appreciation to the International Centre for Theoretical Physics (ICTP) for providing me with the opportunity to present my work, network with other researchers, and participate in workshops organized by the ICTP. These experiences not only enhanced my understanding of DFT but also introduced me to the Quantum Espresso simulation package software, which proved invaluable in my research.

Specifically, I thank Kabarak University for offering an opportunity I will always treasure. Thank you

ABSTRACT

Superconducting magnets have been in demand due to their high magnetic fields and high currents. In high-field magnets, particularly those used in Magnetic Resonance Imaging and the International Thermonuclear Experimental Reactor, as well as in transmission cables, mechanical loading during cool down due to thermal contractions of the material is very large. This can lead to poor performance of Niobium-Tin since it is a major component of the magnetic coils, whose superconducting performance is affected by pressure. Similarly, Niobium Tin made by the internal tin process during fabrication still has significant potential in performance. To achieve this potential, the concept was re-examined and optimized for the future needs of High Energy Physics. The idea in this thesis originated from re-examining the concept of internal tin, recognizing what has been learned on its strengths and weaknesses, and using that knowledge to propose a high-performance conductor suitable for various strains and conditions, while still maintaining its high current density. Niobium-Tin was doped with Titanium, and the end product was subjected to pressure to study how much strain it can withstand. The study reveals that Niobium Tin is dynamically stable and brittle, and highly susceptible to pressure-induced changes, while Titanium-doped Niobium Tin shows enhanced resistance to deforming stress. These outcomes indicate that Titanium doping significantly improves the mechanical robustness and overall performance of the conductor under pressure. The study reports the electronic structure and elastic properties, which provide information on the material's stability, dynamic properties, and pressure-induced superconducting properties of Niobium-Tin and Titanium-doped Niobium-Tin (Ti; Nb3Sn). The study was conducted using a computational method, specifically the Density Functional Theory Method, and applied the open-source software Quantum ESPRESSO code. Niobium Tin is a superconductor. The key outcome is that Titanium-doped Niobium Tin is a better-performing conductor compared to undoped Niobium Tin under mechanical stress, suggesting it is more suitable for practical applications in superconducting magnets. An experimental study of the effect of pressure on Niobium Tin and Titanium-doped Niobium Tin is recommended.

Keywords: *High Energy Physics, Electronic Structure, Dynamical properties, Elastic Properties, Density Functional Theory*

TABLE OF CONTENTS

LIST OF TABLES

LIST OF FIGURES

LIST OF ABBREVIATIONS AND ACRONYMS

BCS – Bardeen-Cooper-Schrieffer

CHPC – Centre for High Performance Computing

CICC – Cable-in-conduit conductors

DFT – Density Functional Theory

Ecut – Plane wave cut-off energy

ESPRESSO – Open-Source Package for Research in Electronic Structure, Simulation and Optimization

Exc – Exchange and Correlation energy of an interacting system

GGA – Generalized Gradient Approximation

GRACE – Graphing Advanced Computing and Exploration of data

ITER – International Thermonuclear Experimental Reactor

LDA – Local Density Approximation

MRI – Magnetic Resonance Imaging

Nb_3Sn – Niobium-Tin

NMR – Nuclear Magnetic Resonance

PBE - Perdew-Burke-Ernzerhof

Pwscf – Plane-Wave-Self-Consistent Field

QE – Quantum Espresso

Ti: Nb_3Sn – Titanium Doped Niobium-Tin

USPP – Ultra soft pseudo potentials

∇ – Gradient operator/Laplacian operator

Vexc – External potential

XcrysDen – X-window Crystalline Structure and density

ψ – Many-electron wave function

ϕ – Coulomb potential

CONCEPTUAL OPERATIONAL DEFINITION OF TERMS

Superconductivity: A physical phenomenon in which certain materials, when cooled below a specific critical temperature, completely lose their electrical resistance. This means that electric current can flow through them indefinitely without any energy.

Density Functional Theory or **DFT**: This is a quantum mechanical method that allows researchers to explore the electronic structure of atoms, molecules, and solids. Instead of trying to track each electron individually—a task that becomes overwhelmingly complex for many-body systems DFT focuses on the electron density, a simpler quantity that still captures the essential physics. This makes DFT both powerful and computationally efficient for investigating how materials behave at the atomic level.

Quantum ESPRESSO: It is an open-source software package designed to model and simulate the electronic and structural properties of materials. Researchers use it to understand how atoms interact, how materials respond to stress or temperature, and how they conduct electricity.

Pseudopotentials: In quantum simulations, Pseudopotentials simplify the model by replacing the core electrons and their interactions with an effective potential that only focuses on the valence electrons, which are most important for chemical bonding and conductivity. This approach speeds up calculations while still providing accurate results for most practical purposes.

Shear Modulus (G): It is the measure of the elasticity and stiffness of a material and is defined as the ratio of shear stress to the shear strain of a material

Electronic Properties: These are representations that are used to describe the behaviour of electrons in a material.

Bulk Modulus: This is the relative change in volume of a material produced by a unit compressive or tensile stress acting over the surface.

Young's Modulus: This is a property of a material that tells us how easily it can stretch or deform and is defined as the ratio of tensile stress (amount of force applied per unit area) to tensile strain (extension per unit length) of a material.

Bulk Modulus: This is the relative change in volume of a body produced by a unit compressive or tensile stress acting uniformly over the surface of a material.

Anisotropy Factor (E): This is the average of the cosine of the scattering angle θ and has a probability density with a single scattering direction as a parameter.

CHAPTER ONE

INTRODUCTION

1.1 Introduction

This section gives a brief background of the study.

1.2 Background of the Study

Superconductivity is a phenomenon in which a material is able to conduct current with zero resistance at very low temperatures (Kamerlingh Onnes, 1911). Onnes was awarded the Nobel Prize for his work in 1913. Many metals possess this property, but very few of them have all the characteristics suitable for magnet design. It was not until much later (following advances in quantum physics and mechanics) that the complete microscopic theory of superconductivity was presented by Bardeen, Cooper, and Schrieffer (1957). Their theory, known as the Bardeen-Cooper-Schrieffer theory, explained the flow of current without resistance by the introduction of the key concept of Cooper pairs, which are pairs of electrons interacting through the exchange of phonons inside the crystal lattice.

Niobium Tin (Nb_3Sn) was one of the first ever known superconductor compounds. It forms a major area of interest due to its unique properties that make it have applications in important areas such as medicine and the nuclear industry. It is used to make Magnetic Resonance Imaging (MRI), transmission cables, and the International Thermonuclear Experimental Reactor. The MRI machines help in patient diagnosis without performing unnecessary surgery. Most Flux Quantized transmission cables help in transmissions of high frequency (energy), which require superconductors. Due to the zero-resistance offered by superconductors, power loss is minimized, resulting in minimal costs (Marzi G *et al*, 2005).

Niobium Tin is a superconductor that is majorly affected by mechanical loading. Studies show that most strains lead to low performance of Nb_3Sn. The effects of hydrostatic pressure and uniaxial strain have been studied in Nb_3Sn, revealing a low-performance effect (Marzi G et al., 2005). The report indicates that Nb3Sn wires are inserted into stainless steel conduits, where compressive stresses arise due to the differing thermal contraction coefficients of the materials.

Titanium (Ti) doped Niobium-Tin is a better version of Niobium-Tin due to its high current density. The conductivity of pure Nb and Ti in Sn achieves 2700 A/mm2 at 12 T (Bruce A. Zeitlin, 2005). Due to its superior properties compared to Niobium-Tin, pressure may have a less significant impact on its performance. Therefore, a study comparing the pressure effects on both Niobium-Tin and doped Niobium-Tin is expected to guide the optimal choice for improved performance in various applications.

Studying critical and transmission temperatures under various external pressures for doped and undoped Niobium-Tin should bring a clear understanding of material fabrication and design. This will help manufacturers develop strain-tolerant systems that offer improved performance. Dynamical and structural properties are necessary parameters of a crystal that help in laying the foundation for research.

1.3 Statement of the Problem

Previous studies have examined how mechanical deformation influences the superconducting properties of materials such as Nb_3Sn and Nb-Al. Notably, Smith et al. (2005) experimentally investigated the relationship between hydrostatic pressure and the critical temperatures of these compounds. Their findings revealed that critical temperature is significantly affected by pressure, with Nb_3Sn showing the greatest sensitivity resulting in considerable performance degradation (Zhang et al., 2015). This

presents a major challenge in high-field applications where mechanical stress is unavoidable. The current study aims to address this issue by investigating the superconducting behavior of Nb_3Sn, including the effects of Titanium doping, under varying pressures. The goal is to contribute additional computational insight to existing experimental data, propose more resilient material alternatives, and ultimately help reduce performance-related challenges in industrial applications.

1.4 Objectives of the Study

1.4.1 General Objective

The main objective of this study was to determine computationally the electronic structure of Nb_3Sn and Ti; Nb_3Sn and the effects of applied pressure on the superconducting properties of Nb_3Sn and Ti; Nb_3Sn.

1.4.3 Specific Objectives

i. To determine computationally the electronic structural properties of Nb_3Sn.
ii. To determine computationally the dynamical properties of Nb_3Sn.
iii. To investigate the effect of external pressure on the superconducting properties of Nb_3Sn and Ti; Nb_3Sn using computational methods.
iv. To determine the elastic properties of Nb_3Sn.

1.5 Research Questions

i. What are the electronic structural properties of Nb_3Sn?
ii. What are the dynamical properties of Nb_3Sn?
iii. How are the superconducting properties of Nb_3Sn and Ti; Nb_3Sn affected by external pressure?
iv. What are the elastic properties of Nb_3Sn?

1.6 Justification of the Study

The findings of this study will contribute to the understanding and development of strain-tolerant superconducting systems, offering a pathway to significantly enhance the performance and operational reliability of devices such as MRI machines, particle accelerators, and fusion reactors, where mechanical loading is unavoidable. Unlike conventional approaches that focus solely on improving critical temperature or current density, this research addresses the often-overlooked issue of mechanical strain, providing a more holistic and durable solution for industrial applications. By guiding material selection and design, the study has the potential to reduce maintenance costs, extend device lifespans, and support the development of next-generation superconducting technologies.

1.7 Significance of the Study

Computational studies of the effect of external pressure on Nb3Sn and Ti will help develop knowledge on how these materials respond to mechanical stress. This will help manufacturers develop strain-tolerant systems that offer improved performance. Learning the critical and transmission temperature under varying external pressure will lead to more efficient systems in the market.

1.8 Scope of the Study

This study investigates the electronic structure and pressure-dependent superconducting properties of Niobium-Tin (Nb_3Sn) and Titanium-doped Niobium-Tin (Ti: Nb_3Sn) using advanced computational modeling techniques. The primary focus is to understand how the application of external pressure influences the structural, electronic, and superconducting behavior of these materials specifically their critical temperature (Ti), which is a key indicator of superconducting performance.

To achieve this, the study employs first-principles calculations based on Density Functional Theory (DFT), implemented through the Quantum ESPRESSO open-source simulation package. This computational approach allows for an in-depth exploration of the materials at the atomic and electronic levels, without relying on experimental data.

The scope includes:

- Modelling the unit cell structure of both Nb_3Sn and Ti: Nb_3Sn.
- Calculating the electronic band structure to determine metallic behavior.
- Evaluating phonon dispersions to confirm dynamical stability.
- Calculating elastic constants to assess mechanical stability under varying pressure.
- Determining critical temperature changes in response to pressure.
- Comparing the pressure resilience of pure and doped compounds to identify material improvements due to Titanium doping.

Through this comprehensive computational study, the work aims to contribute to the design of more mechanically robust and pressure-tolerant superconducting materials for practical applications such as high-field magnets, fusion reactors, and advanced cryogenic systems.

1.9 Assumptions of the Study

i. The quantum espresso code that was used carried out an effectively quantum analysis to determine the desired properties.
ii. The data and information for reference on the properties of Niobium Tin and other similar works would be available.
iii. The time to carry out the research would be enough to come up with the desired results that would give answers to the stated objectives.

CHAPTER TWO

LITERATURE REVIEW

2.1 Introduction

Some studies on the properties of Niobium Tin have been done. This chapter provides insight into the behavior of Nb3Sn and Ti-Nb3Sn under various conditions, including uniaxial strain and hydrostatic pressure, as reported by several scholars. A clear conceptual framework and the research gaps are also highlighted.

2.2 Related Studies on Niobium Tin

2.2.1 Superconductivity

Kamerlingh Onnes, in 1911, discovered the Superconductivity of materials, that is, the ability of a material to conduct DC electric current with zero resistance when cooled below its critical temperature (Tc). Dirk Van Delft (1911) therefore called the phenomenon superconductivity. This property of conducting electric current makes the superconductor useful in hospitals for Magnetic Resonance Imaging (MRI), particle accelerators, generation of strong DC magnetic fields, and cables for power transmission, to mention a few. Therefore, more studies had to be done to improve the superconductivity of materials.

2.2.2 Electronic, Structural, and Elastic Properties

Recent studies have delved into the electronic and structural properties of Nb_3Sn under various conditions. Wu et al. (2023) employed first-principles calculations to investigate the electronic properties, phonon dispersion, electron–phonon coupling, and superconducting gap of Nb_3Sn under hydrostatic pressure up to 9 GPa. Their findings indicate that both the charge density wave (CDW) and superconducting orders respond to pressure, with transition temperatures suggesting a complex interplay between structural instability and superconductivity.

Poirier et al (1984) measured the elastic constants of polycrystalline Nb_3Sn between 4.2 and 300 K using an ultrasonic pulse propagation technique. The study found that both shear and Young's moduli soften dramatically upon cooling to the superconducting temperature, with no abrupt change near or below the martensitic phase transformation at 43 K. Poisson's ratio also changes considerably on cooling, highlighting the material's sensitivity to temperature variations.

These studies underscore the importance of understanding the electronic and elastic properties of Nb_3Sn under varying conditions to predict its behavior in practical applications.

2.2.3 Effect of Pressure on Niobium Tin

The impact of hydrostatic pressure on Nb_3Sn has been a subject of extensive research. Zhang et al. (2015) determined that elastic moduli, including bulk, shear, and Young's moduli, increase with hydrostatic pressure. However, they also noted that the critical temperature of Nb_3Sn decreases under pressure, indicating that mechanical strains significantly affect superconducting properties

Marzi Rui et al. (2023) experimentally investigated the mechanical behavior and strain sensitivity of Nb_3Sn, revealing that the strain sensitivity has a microscopic and intrinsic origin. They observed shifts in the Nb_3Sn critical surface, suggesting that pressure-induced changes in the material's microstructure can influence its superconducting properties.

These findings emphasize the need for a comprehensive understanding of how pressure affects Nb_3Sn to optimize its performance in high-field applications.

2.2.4 Studies on Doped Niobium Tin and Related Compounds

Doping Nb_3Sn with elements like titanium has been explored to enhance its superconducting properties. Morita et al. (2021) reported that Ti doping improves the microstructure of Nb_3Sn, promoting Nb_3Sn layer formation and enhancing superconducting characteristics. They found that doping Ti into the Cu-Sn matrix was more effective than doping into the Nb core, as it led to a thicker Nb_3Sn layer and better superconducting performance. These studies suggest that doping Nb_3Sn can improve its structural integrity and superconducting properties, making it more suitable for practical applications.

2.2.5 Impact of Mechanical Loading on Superconducting Performance

Mechanical loading during cool-down and operation can significantly affect the performance of Nb_3Sn -based superconductors. Rack et al. (2018) reported irreversible critical current degradation upon mechanical loading, stating that mechanical degradation due to loading is a limiting factor in most Nb_3Sn superconductors.

Chiesa (2009) highlighted that the Cable-in-Conduit Conductor (CICC) design, currently standard for large magnets, has inherent mechanical weaknesses. Each strand is not completely supported and can experience large loads during operation, leading to performance degradation. Additionally, Chiesa emphasized the importance of balancing cost and difficulty of assembly with factors like stability against mechanical disturbances, efficiency of the coolant used, protection of the conductor, and mechanical stability of the conductor and supporting structure.

These insights underscore the critical role of mechanical behavior in determining the performance of Nb_3Sn -based superconductors and the need for designs that mitigate mechanical stresses.

2.2.6 Summary

Recent studies have provided valuable insights into the effects of pressure and mechanical loading on the superconducting properties of Nb_3Sn. Understanding these effects is crucial for optimizing the performance of Nb_3Sn -based superconductors in practical applications. The integration of doping strategies and advanced designs can further enhance the resilience of the material to mechanical stresses, paving the way for more efficient and reliable superconducting devices.

2.4 Conceptual Framework

Figure 1

Conceptual Framework

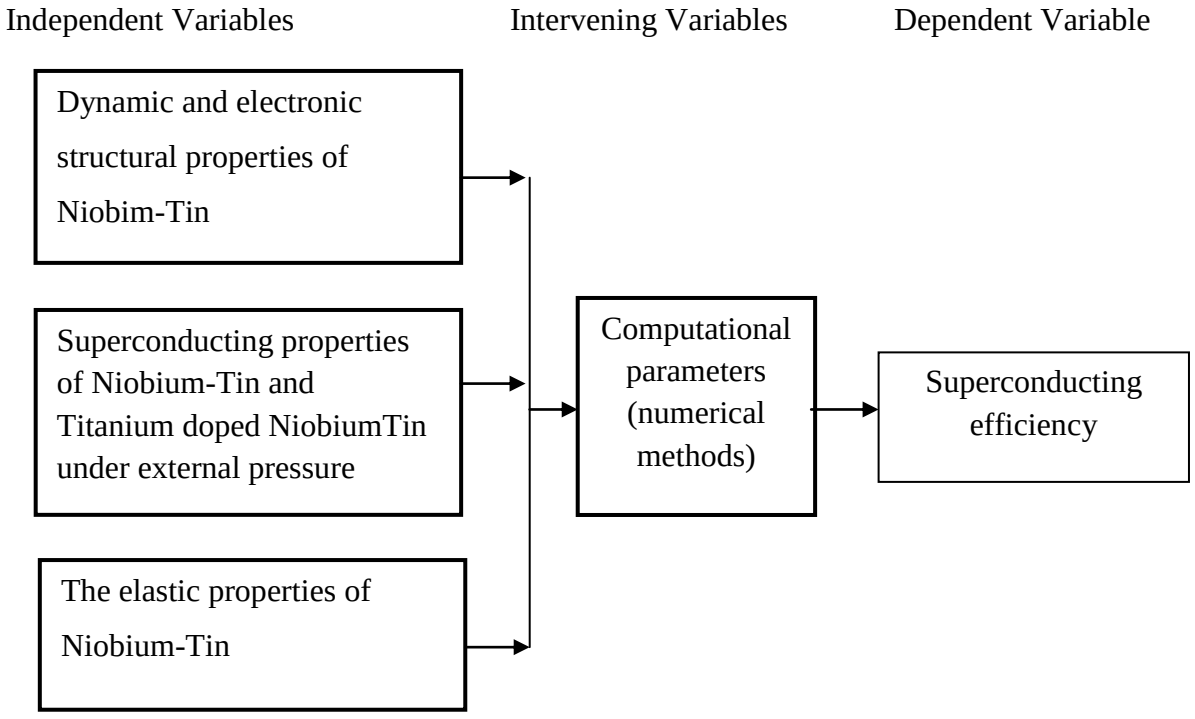

Source: Author, (2025)

Figure 1 illustrates the conceptual framework. There are three sets of variables: dependent, independent, and intervening variables. Independent variables are dynamic properties, electronic structure, and mechanical properties under pressure.

The dependent variable is the superconductivity efficiency. Computational codes, which are solutions to the Schrödinger equation, serve as intervening variables, helping to explain the various independent variables. The structural optimization will be achieved through relaxation using an input file and implemented in Quantum Espresso for self-consistent fields. Electronic structure calculation is performed using the desired K-points, which provides the density of state calculation.

2.5 Research Gaps

The study directly addresses the gap highlighted by Chesa L (2009), who identified four critical issues affecting magnet stability mechanical, electromagnetic, nuclear, and thermal disturbances as well as the importance of conductor protection and mechanical integrity. While Chesa emphasized the need for improved stability in superconducting materials, particularly under external disturbances, he did not provide a specific material solution or detailed mechanical analysis to address these vulnerabilities.

This study builds upon that foundation by proposing a modified version of Niobium-Tin doped Niobium-Tin as a potential solution to improve stability, particularly under mechanical stress. To fill the identified gap, the current research focuses on mechanical stability, a key area outlined by Chesa, and evaluates the material's performance by calculating its elastic constants. These constants are critical indicators of how the material responds to stress and deformation, and thus provide a quantitative basis for assessing its mechanical robustness.

By proposing a material innovation and subjecting it to rigorous mechanical evaluation, the study not only responds to the issues raised by Chesa but also moves a step forward in designing superconductors that are better suited to withstand the operational demands of advanced magnet systems.

CHAPTER THREE

RESEARCH DESIGN AND METHODOLOGY

3.1 Introduction

This chapter gives the design in which the research was done, how the data was collected, and how the data was analysed.

All the calculations in this work were done using the Quantum Espresso computer code, which is multi-purpose, multi-platform software for ab initio calculations of periodic and disordered condensed matter systems. Quantum Espresso stands for Quantum-open-Source Package for Research in Electronics, Simulations, and Optimization.

Computational modelling describes the properties of matter based on equations. Computer simulation is realized by running computer programs implemented in the Quantum Espresso code. Thus, the study described how Quantum Espresso operates and derived the mathematical equations solved by the software based on Density Functional Theory. The electron-ion potential was described by means of Vanderbilt's Ultrasoft Pseudo Potentials (USPP). USPPs are transferable and smooth, as mentioned earlier, ensuring rapid convergence in the calculated total energy of the system. This, in turn, achieves rapid convergence of the 18 system properties with respect to an increase in the plane wave basis set. The PBE form of the GGA pseudo potential was used to treat the exchange and correlation energies in electronic structure calculations.

Quantum espresso software is suited for first-principle calculations and modelling, and it is written in the Fortran language. Espresso is an acronym for Open-Source Package for Research in Electronic Structure, Simulation, and Optimization, based on Density Functional Theory (DFT), plane wave basis sets, and also on pseudo potentials.

The plane wave DFT functions of QE were provided by the plane-wave self-consistent field (PWscf), a set of programs for electronic structure calculation within DFT that uses plane wave basis sets and pseudo potentials. These PWscf were used to solve the self-consistent scheme of Kohn-Sham equations obtained for a periodic solid, to carry out total energy calculation, and post-processing, which allowed data analysis and plotting.

Quantum espresso helps calculate the ground-state energy and one-electron Kohn-Sham orbitals to be able to find atomic forces, strains, and optimization of structures. The data runs programs such as scf, nscf, density of states, and bands to get the band structure. It also aids in optimization of K points, Cutoff energy, and Symmetry points. The PWscf modules supported by the software include thermo_pw.x, pw.x, q2r.x, and ph.x for the input data and pp.x for post-processing.

The codes for data post-processing in pp.x extract the specified data from files produced by pw.x and prepare it for plotting by writing it into formats readable by plotting programs. These programs include bands.x, plotband.x, dos.x, Ph.x and lambda.x. The bands.x extracted files produced by pw.x that were necessary for band structure plotting. Plotband.x read the output of bands.x, producing band structure plots, while dos.x calculated the electronic Density of States (DOS). Ph.x calculated the phonon dispersions and lambda.x calculated the Superconducting transition temperature.

3.2 Superconducting Properties

We used a combination of standard methods with newer machine-learning methods. Specifically, density functional perturbation theory was employed to calculate the electron–phonon properties. For the machine learning, it was chosen due to its algorithms that not only have the ability to predict the relevant physical properties, such as the electron–phonon coupling strength, λ, and the averaged phonon frequency, but also are capable of providing an interpretation of the data. The values of the electron–

phonon coupling strength and phonon frequency are not completely independent. In fact, systems with soft phonons, i.e., materials close to structural instabilities, will often exhibit large values for the electron–phonon coupling constant, leading to a degree of anti-correlation between electron–phonon coupling strength and phonon frequency. Phonon frequency increases monotonically with increasing pressure, although in a sublinear way.

For the calculation of the superconducting properties, we used the Perdew–Wang local-density approximation Perdew *et al.*, (1992). Our choice was based on the fact that the local-density approximation performs surprisingly well when compared, for example, to several commonly used generalized gradient approximations Li *et al.*, (2014), and is more stable numerically. In any case, to understand the dependence on the results with the functional, the PBE functional was used for a few compounds for the q-sampling of the phonons.

3.3 Superconducting Transition Temperature

The superconducting transition temperature calculation was based on the McMillan equation of superconducting transition temperature developed from Eilenberg's theory. The values of λ and phonon frequency were then used to calculate the superconducting transition temperature.

$$T_C = \frac{\theta_D}{1.45} \exp\left[\frac{-1.04(1+\lambda)}{\lambda - \mu^*(1+0.62\lambda)}\right] \quad \text{..... (1)}$$

The strength of a material can be explained on the basis of phonons in a crystal lattice structure. These modes of vibration decrease the forces acting on the displaced atoms from the equilibrium position of symmetry. This results in a decrease in the frequency of their oscillation. This effect leads to lattice distortions that are periodic in nature, resulting in a lowered energy of the crystal and a negative energy distribution to the soft

phonons. In this case, the criterion for crystal stability is associated with phonon frequencies, and instability can occur depending on the magnitude of distortions.

3.4 Phonon Dispersion

Phonon calculations for each structure were performed with a (10 × 10 × 10) q-point grid to sample the Brillouin zone. The dynamical matrices were calculated on a (4 × 4 × 4) grid, and Fourier interpolation was used to calculate phonons for any chosen q-point. Koretsune T and Arita (2017) study of phonons assists in understanding properties of materials such as thermal and electrical conductivity. A phonon refers to a kind of lattice vibration in a crystal, where the particles vibrate at the same single frequency. From the phonon dispersion calculation, one can deduce the critical temperature of the material under study.

A dispersion relation refers to the relationship between the frequency of vibration and the wave vector. It is given by the following relationship:

$\omega = (\boldsymbol{k})$ Where k is the wave vector, ω is the frequency of vibration. .....(2)

The superconducting transition temperature was based on the McMillan equation of superconducting transition temperature developed from Eliashberg theory within BCS theory (Dynes et al., 1972).

3.5 Debye Temperature

The Debye temperature, Debye Vibrational energy, Debye Vibrational free energy, Debye Entropy, and Debye heat were obtained by Quantum Espresso Simulation Package with the calculation by thermo_pw.

The Debye temperature is an important quantity that correlates with many physical properties of solids, such as specific heat capacity, elastic constants, and superconducting

temperature (Ravindran *et al*, 1998). One of the standard methods to calculate the Debye temperature can be estimated from the averaged sound velocity (Zhang *et al*., 2007). The average sound velocity V_M is approximately given by;

$$Vm = \left(\left[\frac{1}{3}\left(\frac{2}{v_t^3}+\frac{1}{v_l^3}\right)\right]\right)^{-1/3} \quad \ldots(3)$$

Where V_t and V_l are the longitudinal and transverse sound velocities, respectively, which can be obtained from bulk modulus B and shear modulus G (Wang & Ye, 2003).

$$V_t = \left(\frac{3B+4G}{3\rho}\right)^{1/2}$$

$$V_t = \left(\frac{G}{\rho}\right)^{1/2} \quad \ldots (4)$$

The values of Debye temperature are estimated using;

$$\Theta_D = \left(\frac{h}{K_B}\left[\frac{3nN_{AP}}{4\pi M}\right]\right)^{-1/3} V_M \quad \ldots.(5)$$

Where V_M is the average sound velocity, p, k_B and N_A are Planck's constant, Boltzmann constant, and Avogadro number, respectively. ρ is the density, M is the molecular weight, and n is the number of atoms in the unit cell.

3.6 Electronic Structure Properties

The density functional theory (DFT) has successfully been applied to the ab initio calculations of the ground-state properties. In view of these circumstances, the calculations were based on the plane wave self-consistent field (PWscf) method as implemented in the Quantum Espresso Simulation package. The PWscf can lead to very accurate results comparable to other all-electron methods. For the exchange correlation

functional, the Generalized Gradient Approximation (GGA) according to Perdew, Burke, and Ernzerhof (PBE) parameterization was used. Optimized cell dimensions, k-points, and kinetic energy cut-off values were determined through graphing, yielding proper values at convergence of the ground state energy.

For structural properties, the lattice constants were calculated by fitting the energy-volume relation to the Murnaghan equation of state (Murnaghan, 1944). It refers to the dimensions of a unit cell. Knowledge of lattice constants is crucial for growing thin layers of materials on other materials, as differences in these constants introduce strains into the layer, preventing the epitaxial growth of thicker layers without defects (Niu and Mueller, 2016).

3.7 Elastic Properties

The elastic properties were used to analyse the stress behaviour and even the deformation of solid layers. This was investigated computationally by the stress-strain-based method. The elastic constants were obtained by calculating the total energy by displacing ions from the ground state as a function of appropriate lattice deformation.

The elastic strain energy was obtained by calculating the full elastic constants, which help in the complete mapping of Young's and shear moduli and Poisson's ratios along all crystal orientations to assess the anisotropies in them. Calculations of Poisson ratios, Young, Bulk, and Shear Modulus (all in Voigt-Reuss-Hill approximations), a useful scheme by which anisotropic single-crystal elastic constants can be converted into isotropic polycrystalline elastic moduli. Elastic constants, average Debye sound velocity, solid density, and Debye temperature were calculated using Thermo_ PW code interfaced with Quantum Espresso.

3.8 Many-Body Problem

Electrons and the nuclei behaviour of materials determine most of their properties in condensed matter. They provide data on bulk moduli, electronic, structural, and mechanical properties. However, it becomes a challenge to solve the Schrödinger equation for a system of many interacting electrons and surrounding nuclei. This is termed the many-body problem. The accurate solution must be determined by considering all these interactions. A number of studies have been carried out to develop a more accurate means to solve the many-body problem. A number of them will be discussed in this section.

To determine the properties of a material from initial studies, one needs to get a solution to the many-body interaction system for electrons and nuclei. (Burke, K *et al*, 2013).

The general Hamiltonian for the many-body problem H, is;

$$H = \sum_i -\frac{\hbar^2}{2M_i}\nabla_i + \frac{1}{2}\sum_{i,j}\frac{z_i z_j e^2}{(R_i - R_j)} - \sum_k \frac{\hbar^2}{2M_e}\nabla_{rk} + \frac{1}{2}\sum_{kj}\frac{e^2}{r_k - r_l} - \sum_{k,l}\frac{Ze^2}{r_k - R_l} \quad . (6)$$

Where;

M_i; represents mass of the nucleus at position R

$M_{e;}$ represents the mass of an electron located at position r_i

Z; represents the atomic number of the atom.

3.9 Born Oppenheimer Approximation

The Born-Oppenheimer describes the nucleus as being heavier than the electron. It therefore moves more slowly than the electrons.

The nucleus and electrons are attracted together by the same magnitude of charge. The nucleus, having a higher mass in comparison to electrons, exerts a smaller velocity,

which is almost negligible. The less massive electrons respond simultaneously to the motion of the nucleus. (Bagayoko, D. 2014).

The equation to be used becomes;

$$\varphi_v(r_i, R_a) = \emptyset(r_i, R_a) \times (R_a) \quad \text{.....(7)}$$

3.10 Hartree-Fork Approximation

This approximation method determines the wave function and energy of a given system in a stationary state. The many-electron problem is reduced to a single-electron problem, and hence, the single-electron problem is solved to obtain the solution for the many-electron problem in this approximation. The N-electrons wave function ψ is expressed as a single determinant of N single-particle wave functions. Since this approximation does not obey the Pauli Exclusion Principle, it is important to incorporate the fermionic nature of the electrons in a many-body wave function so as to build a wave function that is antisymmetrized for the Hartree wave function. This latter wave function changes sign when the coordinates of two electrons are interchanged. (Schleder, G. R.2019).

The Hartree Fock wave function is written as;

$$v_i^{HF}(r) = e^2 \int \frac{n(r') - n_i^{HF}(r,r')}{|r - r'|} dr' \quad \text{... (8)}$$

3.11 Density Functional Theory

DFT concept was developed in 1960s by Hohenberg, Kohn and Sham. Due to the high numerical price of wave function approaches, there was a need to seek alternative approaches to solve the many-body problem. DFT is a standard tool for predicting the electronic properties of materials. In this concept, the electronic density distribution n(r) is considered as the basic property of a many-electron wave function ψ. It follows that

the Hamiltonian is specified by the external potential and the total number of electrons, N, which can be computed from the density simply by integration over all space. This is what formed the basis of the popular Density Functional Theory. (Burke, K *et al,* 2013).

3.12 Hohenberg and Kohn Theorem

Hohenberg and Kohn developed their theorem in 1964 to prove that for a system of interacting particles in an external potential, the external potential is a unique functional of the density. Schleder, G. R *et al* (2019). The ground state energy is therefore determined by

the ground state charge density;

$$E_{Gs} = F\,[n(r)] + \int V_{ext}(r)n(r)dr - \mu\,[\int n(r)d^3\,r - N] \qquad \ldots (9)$$

$F\,[n(r)]$ is the universal functional known as Hohenberg-Kohn functional.

$V_{ext}(r)n(r)dr$ is the external potential

$\mu\,[\int n(r)d^3\,r - N]$ is the ground state electron density

3.13 Kohn and Sham Equation

Kohn and Sham redefined the solution to the many-body problem. They developed a non-existent system of non-interacting particles that gives the same density as any system of interacting particles. They developed the Kohn-Sham potential, a local effective external potential.

A fictitious non-interacting system is constructed such that its density is the same as that of the interacting electrons. The solutions of the Kohn–Sham are single-electron wave functions that depend on only three spatial variables. The Kohn-Sham is taken to be exact because it gives a ground state density as that of the actual system (Kohn, 1999).

The exact ground state density can be written as the ground state density of a fictitious system of non-interacting particles, expressed as follows:

$$[\eta(r)=E_k[\eta(r)]+E_{e\text{-}e}[\eta(r)]+U_{e\text{-}i}[\eta(r)]+E_{XC}[\eta(r)] \quad \text{... (10)}$$

Where:

$E_k[\eta(r)]$ *is the kinetic energy of the electrons,*

$E_{e\text{-}e}[\eta(r)]$ *is electron-electron energy*

$U_{e\text{-}}[n(r)]$ *electron-ion interaction potential*

Figure 2

Flow Chart for Solving the Kohn-Sham Equation.

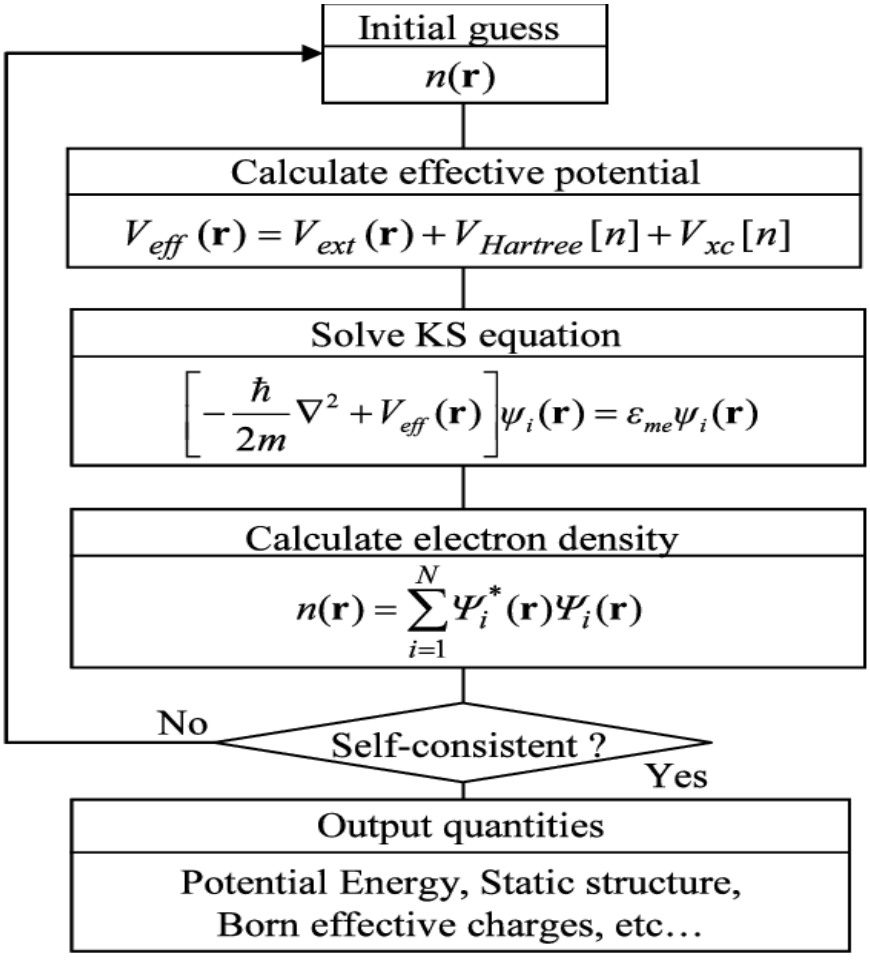

Source: Bickelhaupt, F. M et al (2000)

An electronic charge density n(r) is guessed that gives the minimum energy, that is, minimizes the energy. The density, which is a function of r, is computed and then used as the initial guess for another function, n(r).

The guessed density and the calculated density were found to be the same, indicating that self-consistency had been achieved. The energy could then be calculated. If the calculated density and the guessed density were not the same, a new guess for the density could be made based on the previous step's charge density, and the whole process is repeated until self-consistency is achieved. The choice of basic sets involves selecting the initial data, which is significantly different from the solution or the optimization of the parameters. This stage determines the choice of the advanced estimation of the crystal grid, as well as the atomic orbitals.

Iljasov et al. (2014) state that the next step involves solving the Schrödinger equation. It is done by determining the density of single-electron wave functions since it is impossible to solve the equation with more than one electron system in an atom. Kravcova et al. (2011) present results that can be used to determine various material parameters, such as the geometrical parameters of a crystal grid and the energy connection between its points, as discussed by Kazakova (2009). The results obtained for the atomic structures from parameter calculations can be used to determine the strength of the material according to Iskandarov et al. (2012). Kravcova et al. (2011) argue that the parameter calculation results can also be used to determine the electron structure properties, the band structure, and elastic properties.

3.13 Exchange-Correlation Theory

It is a quantity in the Kohn-Sham equation. It is responsible for the difference between the exact ground state energy and the energy calculated in the Hartree-Fock approximation, using the non-interacting kinetic energy. (Schleder, G. R *et al* 2019)

$$E_{xc}(n) = T(n) - T_o(n) + U_{xc} \quad \ldots (11)$$

T (n) is the exact Kinetic energy functional

T_o (n) is the non-interacting Kinetic energy functional

U_{xc} is the interaction of the electrons

In practical Density Functional Theory codes, some approximations are used for the exchange-correlation functional. The commonly used are the Local Density Approximation and the Generalized Gradient Approximation functional.

3.14 Local Density Approximation

LDA is the oldest exchange-correlation function. It has proven to generate good results for vibrational frequencies, elastic modulus, and phase stability of many systems. It works on an assumption that the exchange-correlation energy at a point r is equal to the exchange-correlation energy of a uniform gas that has the same density at point r. (Burke, *et al*, 2019)

$$E_{xc}^{LDA}[n(r)] = \epsilon_{xc}^{hom}(n(r))dr \quad \ldots (12)$$

Where, ϵ_{xc}^{hom} is a function of the electron density n(r)

One limitation of LDA is that it cannot exactly predict the magnetic properties of some materials. It equally predicts wrong band gaps of some materials.

3.15 Generalized Gradient Approximation

The GGA uses the spatial variation of the electrons to determine the exchange-correlation energy, and it is expressed as;

$$E_{xc}^{GGA}[n(r)] = \int \epsilon_{xc}(n(r), \nabla n(r)) n(r) dr \quad \ldots (13)$$

In the generalised gradient approximation, a functional form approach is adopted, which ensures the normalisation condition and that the exchange hole is definite.

GGA significantly improves on LDA's description of molecular binding energy – a feature that has led to the widespread acceptance of DFT in the chemistry field. This gives rise to an energy functional that depends on both the density and its gradient but retains the analytic properties of the exchange correlation hole inherent in the LDA. (Schleder, G. R *et al*, 2019).

3.16 The Perdew, Burke, Ernzerhof (PBE) Exchange - Correlation Functional

Perdew, Burke, and Ernzerhof created the PBE-GGA exchange-correlation functional. It tends to overestimate bond lengths in calculations, resulting in a mean error and mean absolute error slightly under 0.01 Å, which is less accurate than the Local Density Approximation (LDA), which achieves a mean error of 0.001 Å. However, for calculating bond energies, PBE is widely used because it significantly reduces the mean absolute error to within the desired chemical accuracy of better than 1 kcal/mol (or 50 meV/atom). This study chose PBE due to its design, which preserves various physical characteristics in both the correlation and exchange components, making it suitable for the strongly localized systems under investigation. Consequently, PBE pseudopotentials were employed for all reported calculations.

3.16 Plane Waves

In this study, Density Functional Theory (DFT) and the Born-Oppenheimer approximation were utilized to address the interactions between nuclei and electrons, transforming the complex many-body problem into a single-particle problem governed by an effective potential for 60 stationary nuclei. Plane waves were chosen because their Eigen states are exact for homogeneous electron gases, not tied to any specific atom. Expanding plane waves within the Kohn-Sham wave function is crucial for calculating the total energy of periodic solids. The solutions to the single-particle Schrödinger equation with a periodic potential conform to Bloch's theorem.

3.17 Energy Cut-off

In this material study, the plane wave basis energy is derived from DFT. The optimization of the cut-off energy was assessed using a consistent k-point mesh. Experimental lattice parameters were obtained from crystallographic databases. The energy cut-off convergence for niobium tin was evaluated. The convergence of the plane-wave energy cut-off and the k-point grid was determined at fixed lattice constants, with atomic positions relaxed at 0 K. The volume was varied while relaxing atomic coordinates, a crucial aspect of every DFT calculation.

Energy cut-off convergence relative to total energy was analyzed by selecting a k-point grid expected to converge, with simulations in Quantum ESPRESSO (QE) conducted by progressively increasing the energy cut-off. The energy cut-off values and corresponding energy outputs in Rydberg were plotted, indicating that cut-off values below 30 Ry are insufficient, suggesting a preference for values above this threshold. However, while higher cut-off energies increase computational cost without enhancing precision, they do not compromise accuracy.

3.18 K-Points

Electronic states are restricted to specific k-points based on the boundary conditions applicable to bulk solids. The density of allowed k-points correlates with the solid's volume. An infinite number of electrons corresponds to infinite k-points, but only a finite number of electronic states are occupied at each k-point. Bloch's theorem simplifies the calculation of these wave functions by reducing them to a finite set of states at discrete k-points.

Electronic wave functions at closely spaced k-points are nearly identical, allowing for the representation of electronic states over a region of k-space using just a single k-point. Thus, only a finite number of k-points are necessary to calculate the electronic potential and total energy of the solid. This study employed the Monkhorst-Pack scheme to automatically generate special k-points, ensuring that the irreducible part of the Brillouin Zone is integrated over a uniformly spaced k-point mesh. After rigorous optimization, the k-point grid was varied across a broad range (from 2x2x2 to 22x22x22).

3.19 Pseudo potential Approximation

To enhance computational efficiency, pseudopotentials are typically used to substitute the core electrons of atoms with an effective potential. Since only valence electrons significantly influence the physical and chemical properties of molecules and solids, the pseudopotential approximation is employed. In this method, core electrons are treated as fixed, and the ion-ion interactions are considered electrostatic. This approach eliminates the need to include atomic core states and their strong nuclear potentials. Instead, a weaker pseudopotential acts on a set of pseudo wave functions rather than true valence wave functions. This decouples the small, computationally intensive length scales of core electrons from the interacting valence electrons that primarily determine structural and chemical properties.

Pseudopotentials effectively capture the role of valence electrons in the electronic structure problem. While core electrons remain largely unaffected by their environment and exhibit rapidly varying wave functions near the nucleus, the wave functions become smoother at greater distances. The wave functions outside the **core** mainly influence the properties of valence electrons. The electronic density of the core cancels itself out, remaining essentially frozen while imposing boundary conditions on the external wave functions.

The many-body problem for valence electrons is thus projected onto an effective energy-dependent Hamiltonian, where nuclear attraction is largely screened by a repulsive term that reflects orthogonality constraints (cancellation theorem). Pseudopotentials are typically much weaker and smoother than the original Coulombic potential. In this work, ultrasoft pseudopotentials were utilized, which partially relax the norm conservation constraint while matching scattering properties over a broader energy range. This approach improves transferability and smoothness, introducing charge augmentation mechanisms to maintain norm conservation and balance valence charge density in the core region.

3.21 Norm-Conserving Pseudo-Potential

Norm-conserving pseudopotentials explicitly treat core electrons, simplifying their representation. Since core electron motion is not periodic, normalization is applied to achieve periodicity, facilitating a Gaussian distribution and quicker convergence. The default value for charge density cut-off (ecut 'rho') is typically used, though slight adjustments can introduce noise, particularly affecting forces and stress.

3.22 Ultra Soft Pseudo-Potential

The original electron distribution in the core is Gaussian. If calculations were performed using this distribution, a large number of plane waves would be required. The introduction of ultrasoft pseudopotentials reduces the necessary plane waves, leading to faster convergence. Ultrasoft pseudopotentials generally offer quicker convergence than norm-conserving ones. When using these pseudopotentials, a charge density cut-off (ecut 'rho') that is 8 to 12 times greater than the plane wave cut-off energy (ecut 'wfc') is often recommended.

CHAPTER FOUR

DATA ANALYSIS, PRESENTATION AND DISCUSSION

4.1 Introduction

This chapter presents data analysis, discussion, and results on the optimization, electronic structural properties, dynamical properties, elastic properties, and the effect of external pressure on the superconducting properties of Nb3Sn and TiNb3Sn, respectively, using computational methods.

4.2 Structure Optimization

4.2.1 Lattice Parameter

The lattice parameter was optimized, and the results are as shown in Figure 3.

Figure 3

Lattice Parameter Optimization Curve

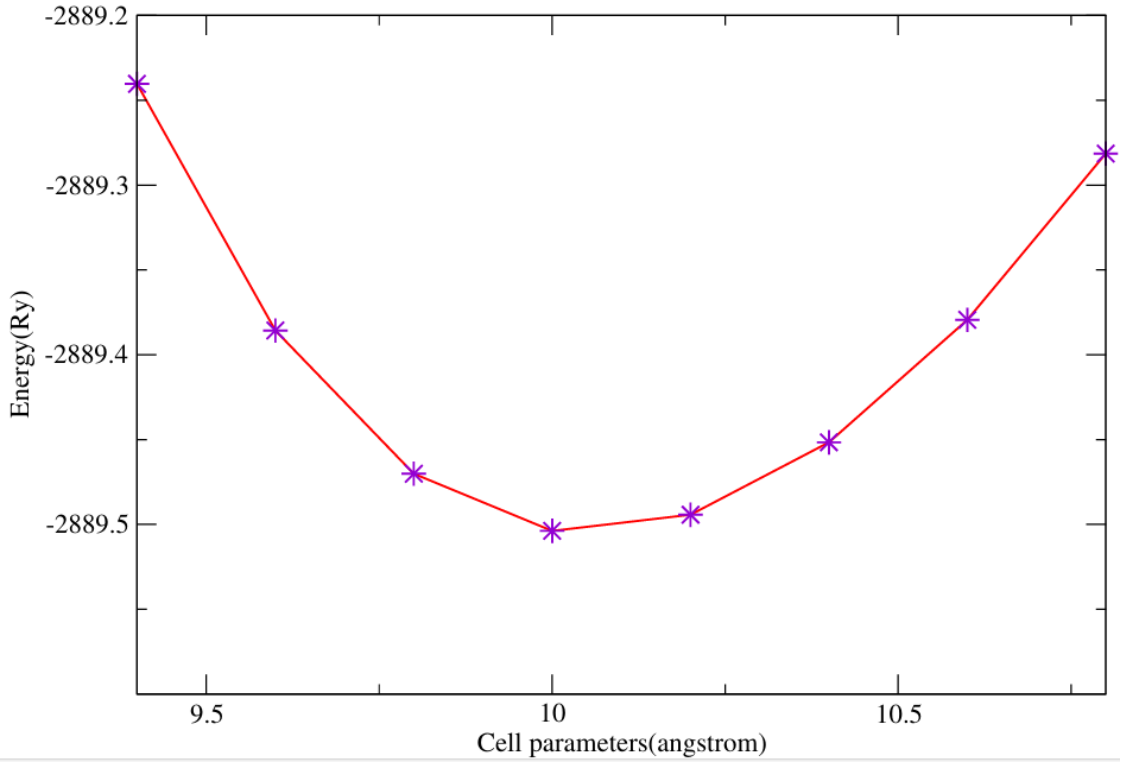

Source: *Computational Work (2024)*

The optimization was done, and accurate values were obtained to be 10.0071Å at convergence.

4.2.2 Energy Cut-Off

The Plane wave basis energy is calculated based on the DFT in the study of a material. The cut-off energy optimization is examined at a constant k-point mesh obtained prior. In this thesis, the energy cut-off convergence for Niobium Tin is shown in Figure 4.

Figure 4

Energy Cut-Off Optimization Curve

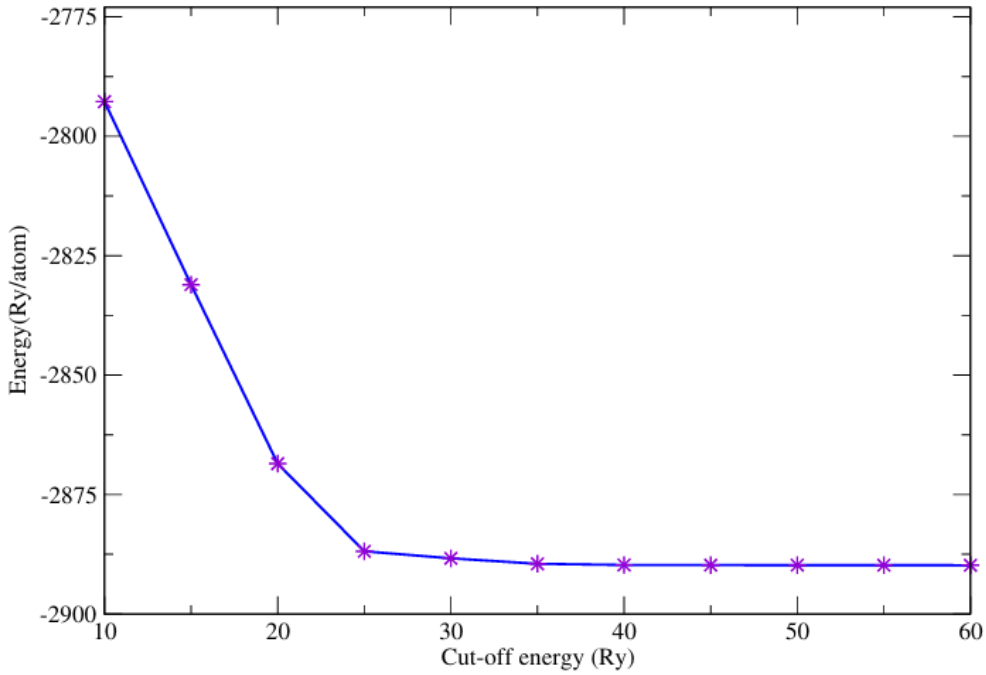

Source: *Computational Work (2024)*

The convergence test of the plane-wave energy cut-off and also the k-point grid was determined at fixed lattice constants, and the atomic position was relaxed at a temperature of 0K. Volume was varied while relaxing the atomic coordinates, a significant principle for every DFT calculation.

The convergence of the energy cut-off in relation to the total energy was determined by choosing a k-point grid for which the results are expected to converge. Then, the system

was simulated in QE by gradually increasing the values of Energy Cut-off. The values obtained for the Energy Cut-off and their output Energy values in Rydberg were plotted as shown in Figure 4 above.The energy cut-off value was calculated to be 40Ry. However, a greater energy cut-off does not increase precision; instead, it increases CPU time, thereby increasing the computation cost, without compromising accuracy.

4.2.3 K-Points

Electronic states are allowed only at a set of k-points determined by the boundary conditions that apply to the bulk solid. The density of allowed k-points is proportional to the volume of the solid. An infinite number of k points accounts for the infinite number of electrons in the solid, but only a finite number of electronic states are occupied at each k-point. The Bloch theorem, which considers periodicity, changes the problem of calculating an infinite number of electronic wave functions to one of calculating a finite number of electronic wave functions at an infinite number of k-points.

The occupied states at each k-point contribute to the electronic potential in the bulk solid so that, in principle, an infinite number of calculations are needed to compute this potential. Electronic wave functions at k-points that are very close together will be almost identical. It is possible, therefore, to represent the electronic wave functions over a region of k-space by the wave functions at a single k-point.

In this case, the electronic states at only a finite number of k-points are required to calculate the electronic potential and hence determine the total energy of the solid. In this study, the special k-points were generated automatically using the Monk Horst-Pack scheme. Monkhorst-Pack scheme ensures that the irreducible part of the Brillouin Zone (IBZ) is integrated over a set (mesh) of uniformly spaced k-points. Following a rigorous optimization process, the k-points grid was varied over a wide range of values (2x2x2 to

22x22x22) since transition metals are known to require large k-point grids. In this thesis, the K-point size after convergence for Niobium Tin was determined to be 10 by 10 by 10.

Optimization of the k-points, lattice parameters, and cut-off kinetic energy was carried out, and the system was run to convergence. Optimization details and graphs are reported in detail. The first step of the computation was to make an input file for the calculations. In our study, the Plane Wave method was used to investigate the electronic and mechanical structure properties of the compound from first principles, using the open-source computer code Quantum-Espresso (Giannozzi et al., 2009).

Self -Self-consistent calculations were run to obtain the total and Fermi energy of the system, which are useful parameters in describing the electronic structure properties of the compound (West, Sun, & Zhang, 2012). The input files were designed such that the mechanical properties, including the Bulk, Shear, and Young moduli, and Poisson ratio, were obtained. Quantum Espresso supports the use of Projector-Augmented Wave (PAW) and Ultra Soft Pseudo Potentials (USPP). Norm-conserving pseudo-potentials are well normalized, a feature useful for an accurate description of bonding in the compound (Hamann, 1989; Hamann et al., 1979).

The 42 PAW Non-Linear Correction Pseudo Potentials were used in these calculations (Dalgarno, Bottcher, & Victor, 1970; Garrity, Bennett, Rabe, & Vanderbilt, 2014; Troullier & Martins, 1991). Before running the Self-Consistent Calculations, the Variable Cell relax(vc-relax) calculation was performed to obtain relaxed atomic positions, and then optimization of cell dimensions, K-points, and the kinetic energy cut off was also done so as to obtain a relaxed crystal structure, to ensure that the ground state crystal structure is obtained and that the results are free from stress(Lund, Orendt, Pagola, Ferraro, & Facelli, 2013; Wales & Scheraga, 1999; Yang et al., 2009). The initial

k-point sampling was done using $2\pi/a$, where a is the lattice parameter (W. Uhoya et al., 2010).

Optimization of the K-points yielded the converged K-points, ensuring a stress and strain-free system. Sampling on the Brillouin zone was done using the Monkhost scheme, and the mesh used was 8x8x6. Exchange correlation was computed by employing the Generalized Gradient Approximation as put forward by Perdew, Burke, and Ernzerhof. A plane wave basis was used as a basis set for optimization of the lattice parameters, k-points, and cut-off kinetic energy so as to obtain converged total energy.

Calculations were performed in the quenched paramagnetic state. The Density Functional Theory, which focuses on the electron density to study the properties of a many-electron body system, was employed. Experimental cell dimensions were used in the input file before optimization. Before optimization was carried out, the variable cell relax calculation was done to obtain relaxed atomic positions, which were then used to perform optimization on the compound.

4.3 Structural Properties

Figure 5

Unit Cell for Niobium Tin

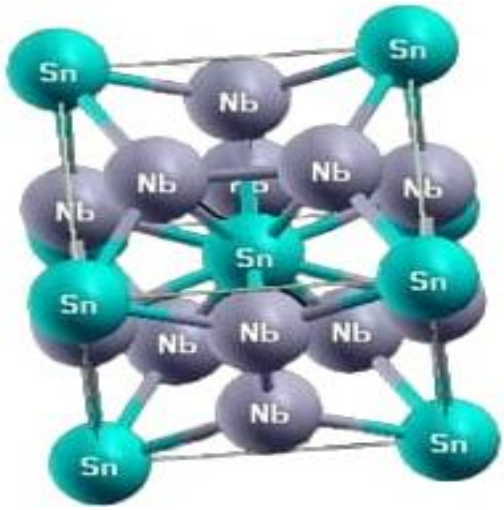

Source: *Computational Work (2024)*

Cubic Niobium Tin has eight atoms per unit cell. The original structure from the database and the optimized structure were simulated using the same values for ecutwfc and ecutrho, and using XCrysDen according to Kokalj (1999), the structures were visualized after optimization. Murnaghan's equation of state was used according to Madsen et al. (2016) for volume optimization by minimizing the total energy with respect to the volume. The Niobium Tin structure was created using XcrysDen software within the Quantum Espresso code to achieve an optimized structure.

4.4 Electronic Properties

4.4.1 Density of States (DOS)

Figure 6

Density of States Graph

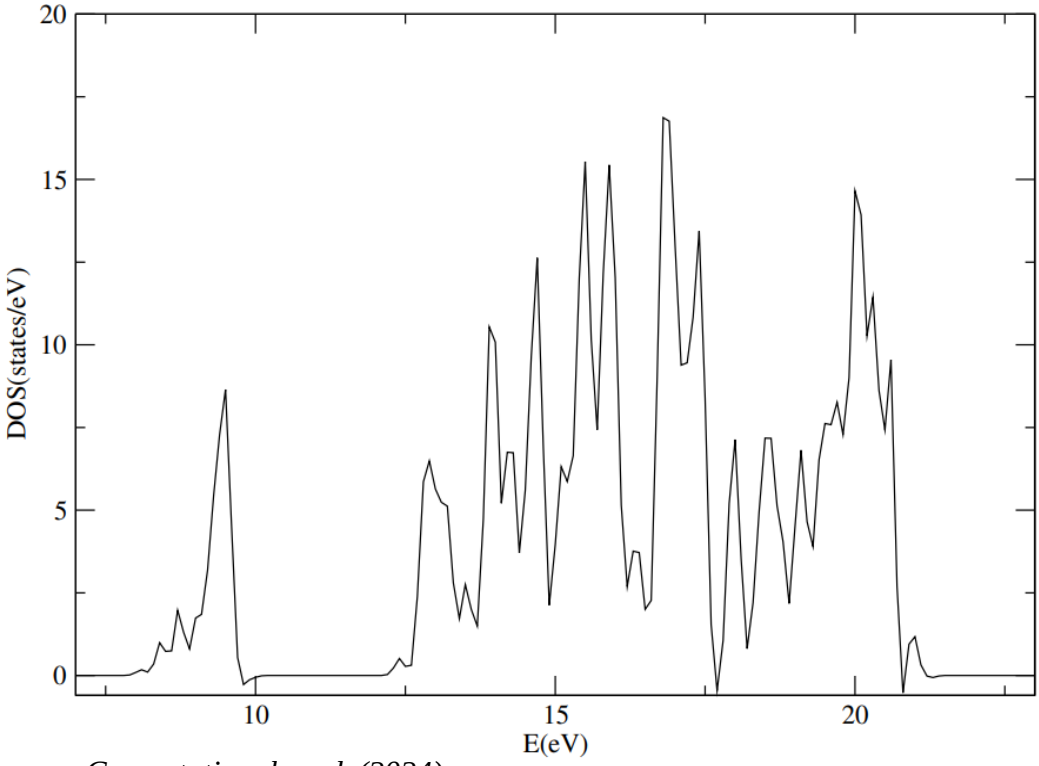

Source: *Computational work (2024)*

To understand the band gap variation of a material, a study of the density of states (DOS) is necessary. The density with long sharp peaks is between energies 9.2eV and 16.7eV. They represent the core electrons that have minimal contribution to determining the properties of the electrons since they are considered to be chemically inert.

4.4.2 Band Structure

Figure 7

Band Structure

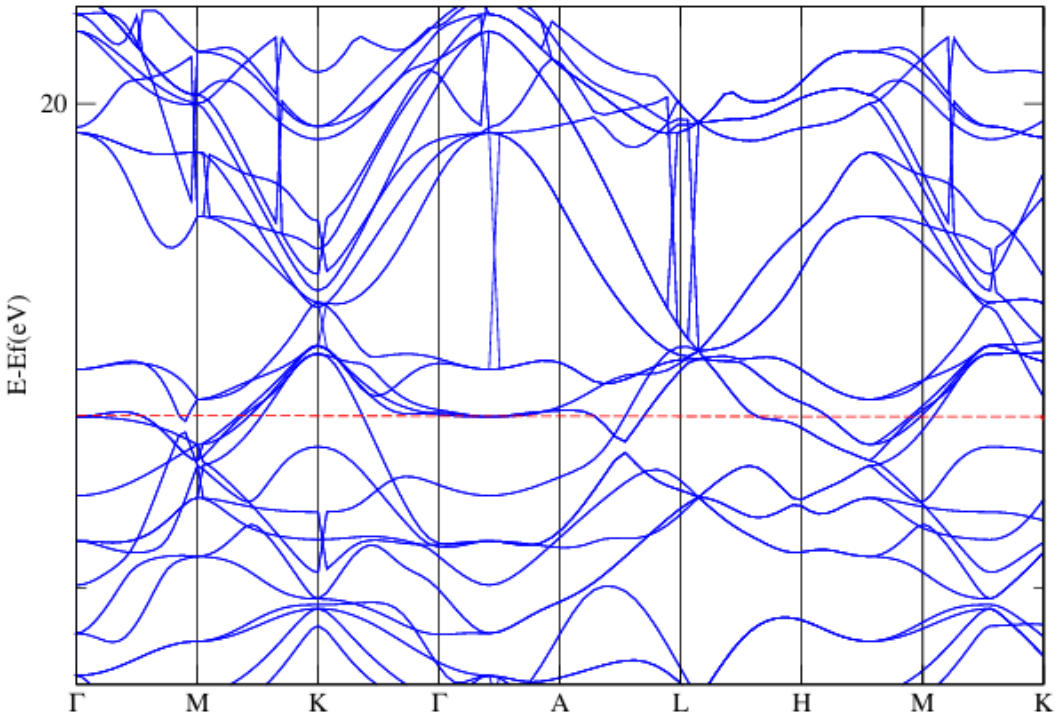

Source: *Computational Work (2024)*

The calculated band structure of Niobium Tin with Ferromagnetic spin configuration along high symmetry directions in the BZ at the ambient pressure is shown in Figure 7. The band structure gives the band gap to be 0.0eV. This clearly shows that the material is a conductor.

4.5 Electron–Phonon Interaction and Superconductivity

Figure 8

Phonon Dispersion Curve

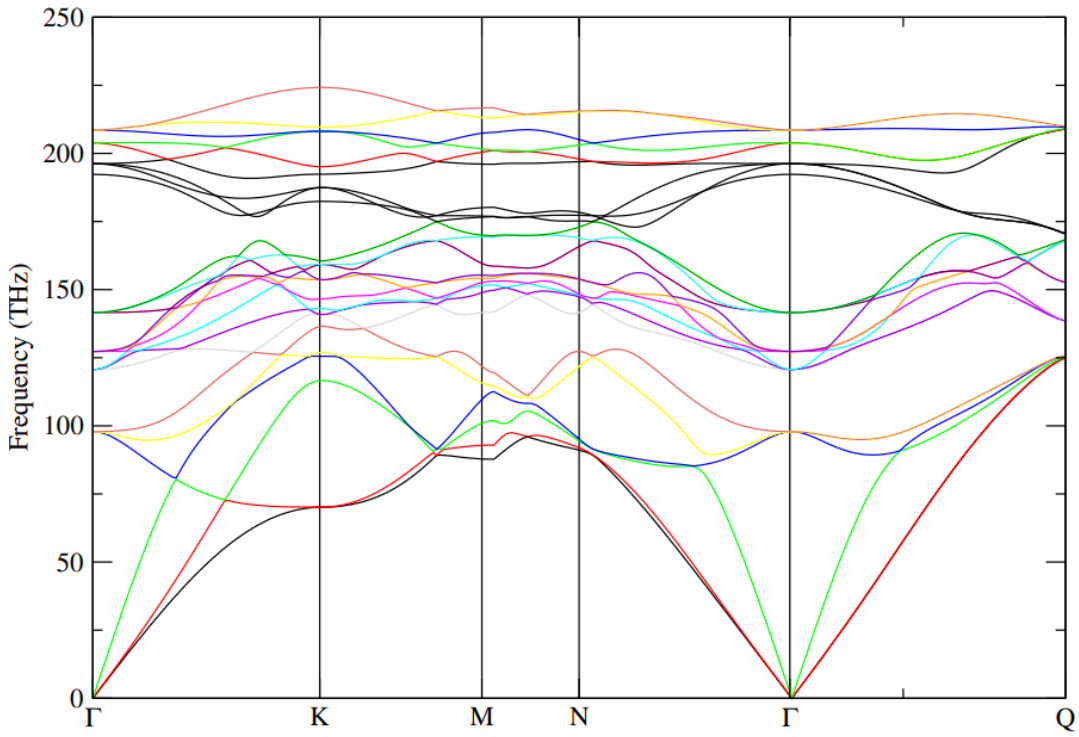

Source: *Computational Work (2024)*

There are two branches in the phonon dispersion relation: the lower mode, which is the acoustic mode, and the upper mode, which is the optical mode. The acoustic mode refers to the in-phase vibration mode, while the optical mode refers to the out-of-phase vibration. The name optical phonon is derived from the fact that the phonons get excited by the infrared radiation in ionic crystals. The phonons were calculated using the Density Functional Perturbation Theory as implemented in PWSCF.

Figure 8 shows the phonon dispersion curve for Niobium Tin. The optical mode and the acoustic mode are clearly differentiated. The acoustic modes are the lower modes converging at the gamma point, as shown in Figure 8, while the optical modes are the upper modes that begin at approximately 100 THz. In the phonon study, there are three

modes that are associated with each mode number n, considering *x*, *y*, and *z*. The number of acoustic modes is usually three for crystals whose number of atoms is equal to or greater than two, and the optical modes are given by the formula 3N-3. Given that Niobium Tin has 8 atoms in its unit cell, there are 24 modes of vibration, 21 being optical modes and 3 being acoustic modes. The acoustic modes converge at the gamma high symmetry point, as shown in the figure.

Acoustic modes vibrate at a slower frequency and are always in the same phase with the unit cell. Optical modes vibrate at a higher frequency compared to acoustic modes. Two adjacent atoms vibrate in a direction opposite to each other in optical modes. In the acoustic mode, the two adjacent atoms will vibrate together in the same direction. Phonon dispersions are computed, and the above information therefore confirms that the compound is dynamically stable.

A system is considered to be dynamically stable at equilibrium if the potential energy is always increasing for any combination of displacement of atoms. The phonons should therefore have non-negative and real frequencies for stability. Negative frequencies imply that the potential energy reduces; hence, the system is unstable. Phonon frequencies arise as a result of the displacement of atoms in a given crystal from their rest position, which in turn makes the forces rise. It is thus important to identify the number of normal modes that are neighboring a certain phonon energy to give details necessary when studying thermal and electrical conductivity, and also establishing the critical temperature of superconducting materials.

In summary, the results of the current study show a fair agreement with the existing data from Sundareswaran *et al* (2010).

4.6 Effects of Pressure on Superconducting Properties of Niobium Tin and Titanium Doped Niobium Tin

Table 1

Critical Temperatures for Niobium Tin and Titanium Doped Niobium Tin under Varying Pressure

	Nb_3Sn	Ti: Nb_3Sn
P(GPa)	T_C (K)	T_C (K)
0	18.6	18.7
2	17.9	18.1
4	17.2	17.7
6	16.0	16.8
8	14.5	15.5
10	13.0	14.2
12	11.0	12.5
14	9.5	11.2
16	8.0	9.8
18	6.5	8.2
20	5.0	6.6
22	2.0	3.9

The corresponding graphs for the behavior of the two materials under varying pressure are shown in Figure 9.

Figure 9

Critical temperature against pressure graph for Niobium Tin and Titanium-doped Niobium Tin

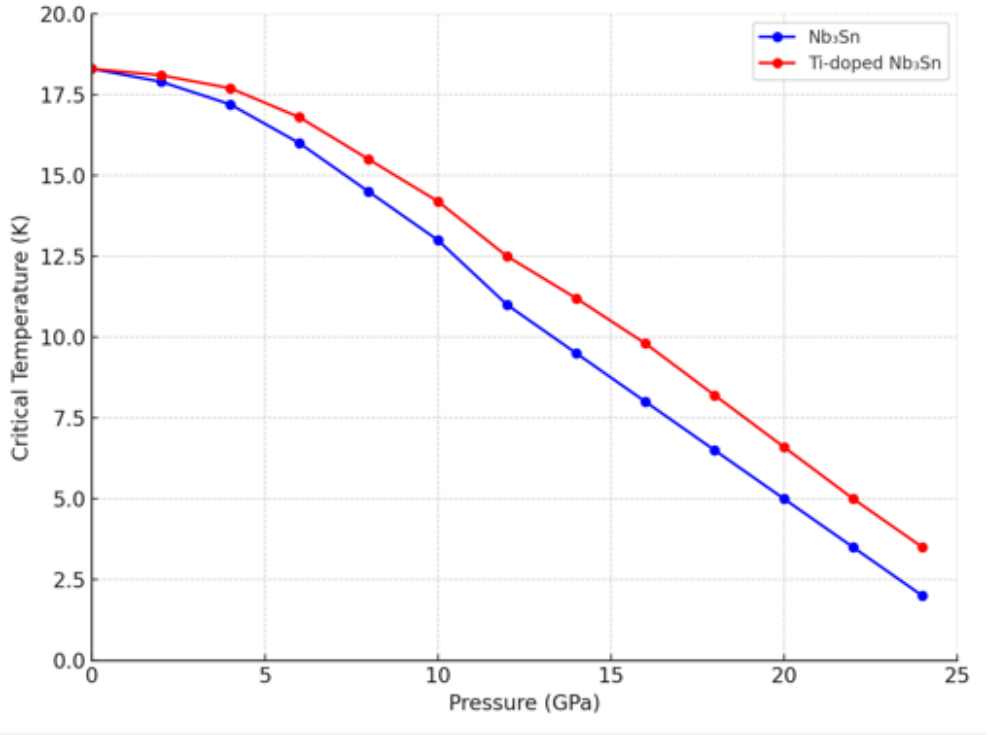

Source: *Computational Work (2024)*

The calculation of the superconducting transition temperature was based on the McMillan equation of superconducting transition temperature developed from Eilenberg's theory given by;

$$T_C = \frac{\theta_D}{1.45} \exp\left[\frac{-1.04(1+\lambda)}{\lambda - \mu^*(1+0.62\lambda)}\right] \quad \text{... (14)}$$

Where Θ_D The Debye temperature, μ*, is the renormalized Coulomb repulsion, and its value is chosen to range from 0.1–0.2, and λ is the electron-phonon coupling constant. The BCS theory was applied in the calculation of the superconducting transition temperature.

The response shows that the Tc maximum in Niobium Tin is 18.65, while the Tc maximum for Titanium-doped Niobium Tin is 18.75. Niobium Tin is a type-II superconductor, whose critical temperature decreases with increasing pressure due to lattice vibration change, affecting the electron-phonon interactions. This leads to a quicker drop in critical temperature. Titanium doping reinforces the structure, helps maintain favorable bonding environments under pressure, hence slowing the decline of T_c with pressure. The reduction in T_c still occurs, but the rate of suppression is less severe due to reduced lattice strain, hence preserving superconducting properties better than undoped Niobium Tin. Titanium helps reduce the pressure sensitivity.

Table 2

Poisson Ratio, Anisotropy Ratio, and Pugh's Index for Niobium Tin and Titanium Doped Niobium Tin under Pressure

	Nb_3Sn			Ti:Nb_3Sn		
Pressure	Anisotropy ratio	Poisson ratio	Pugh's index	Anisotropy ratio	Poisson ratio	Pugh's index
0	0.6833	0.2577	0.577	0.7880	0.2600	0.586
5	0.6943	0.2590	0.579	0.7814	0.2609	0.588
10	0.7001	0.2599	0.587	0.7825	0.2621	0.589
15	0.7111	0.2617	0.596	0.7843	0.2630	0.591
20	0.7444	0.2647	0.599	0.7845	0.2637	0.599
25	0.7543	0.2619	0.581	0.7840	0.2636	0.588

Table 2 compares the responses of Niobium Tin and Titanium-doped Niobium Tin to strains caused by pressure. Materials can change due to intrinsic and extrinsic effects that affect the atomic orientation and structural geometry. This change is highly dependent on the chemical composition, the structure of the crystal lattice, and the deforming stress.

Under pressure, a material undergoes several elastic behaviour changes due to the reduction of interatomic orbitals, which modifies the electronic orbitals and the order of

bonding. If the structure remains unaffected by the loading stress, the electronic properties can, on the other hand, get highly modified. Some of these modifications include: broadening of the band gap, change of the Fermi energy, induction of a semiconductor to conductor change, and change of ordering of the electronic states. Niobium Tin is one type that is highly affected by loading stress, and the effect is less on electronic properties.

Titanium-doped Niobium is more stable to the effects of pressure compared to Niobium Tin, as the changes in application under pressure are minimal. The anisotropy ratio for titanium-doped Niobium Tin at zero pressure is 0.7880. This is a good value of isotropy compared to 0.6833 for Niobium Tin. It indicates that Titanium-doped Niobium Tin has a lower likelihood of producing microcracks under strain circumstances. The Poisson ratio for Titanium doped Niobium Tin is 0.2600, indicating that the material gradually shifts from being brittle to being ductile.

4.7 Debye Temperature

The Debye temperature is an important parameter that correlates with many physical properties of solids such as specific heat capacity, elastic constants, and superconducting temperature (Ravindran *et al,* 1998). One of the standard methods to calculate the Debye temperature can be estimated from the averaged sound velocity (Zhang *et al*., 2007). The average sound velocity V_M is approximately given by;

$$Vm = \left(\left[\frac{1}{3}\left(\frac{2}{v_t^3} + \frac{1}{v_l^3}\right)\right]\right)^{-1/3} \quad \cdots (15)$$

Where V_t and V_l are the longitudinal and transverse sound velocities, respectively, which can be obtained from bulk modulus B and shear modulus G (Wang & Ye, 2003).

$$V_t = \left(\frac{3B+4G}{3\rho}\right)^{1/2} \quad \text{... (16)}$$

$$V_t = \left(\frac{G}{\rho}\right)^{1/2} \quad \text{… (17)}$$

The values of Debye temperature are estimated using;

$$\Theta_D = \left(\frac{h}{K_B}\left[\frac{3nN_{AP}}{4\pi M}\right]\right)^{-1/3} V_M \quad \text{… (18)}$$

Where V_M is the average sound velocity, p, $k_{B,}$ and N_A are the Planck constant, Boltzmann constant, and Avogadro number, respectively. ρ is the density, M is the molecular weight, and n is the number of atoms in the unit cell.

A Debye temperature of above 400 K indicates that the crystal's thermal conductivity is high, while a value below 400K shows low thermal conductivity. Since the compound that was studied had a Debye temperature of below 400 K, it is concluded that Niobium Tin has lower thermal conductivity. For temperatures below the Debye temperature, the heat capacity of the compound increases with the temperature, and for temperatures above the Debye temperature, the heat capacity of the crystal remains constant; it no longer depends on temperature. The Debye temperature and the heat capacity are directly proportional.

4.8 Elastic Properties

Table 3

Elastic Properties

Parameter	Present	Other work (WIEN2K CODE)
C_{11} (GPa)	286.8593	284.23
C_{12} (GPa)	110.0611	107.70
C_{44} (GPa)	60.4042	67.07

From Table 3, it can be noted that the values of elastic constants calculated satisfy the four Born criterion conditions. This therefore shows that the structure studied in this work is elastically stable since it has proven C_{11}-C_{12}>0, C_{44}>0, C_{11}+2C_{12}>0 for structural stability and C_{12}<B<C_{11} for cubic stability.

The study of elastic properties of solids helps in analyzing some of their vital properties such as anisotropy, ductility, and brittleness. The elastic constants are used to show how dynamic and mechanical properties are connected in regard to the type of forces present in the solids. Much emphasis is put on the stiffness and stability of the material. The elastic constants also play a major role in predicting the mechanical nature of solid materials.

A crystal has independent elastic constants depending on the symmetry, and for a cubic structure, there are three such constants, C11, C12, and C_{44}. These constants are obtained by fixing the full energies of a strained crystal to a fourth-order polynomial strain (Pugh, 1954). The bulk modulus is used to measure the ability to resist deformation upon the application of pressure. A greater value of bulk modulus results in a greater capacity to resist deformation (Cherkaev & Gibiansky, 1993). Shear modulus measures the resistance to shear deformation under shear pressure.

The three elastic constants for a cubic crystal structure describe the mechanical hardness of the cubic crystal, and they are required to determine the stability of a given material. C_{11}, C_{12}, and C44 elastic constants are obtained from total energy calculations and signify the single-crystal elastic characters. In contrast, the Voigt–Reuss–Hill approach is a convenient scheme for the elastic constants of materials.

The elastic constants in Voigt notation (C_{ij}) determine the response of a material crystal to external forces. A given crystal cannot be termed stable unless it obeys certain conditions. These constants then play a huge role in determining a material's strength.

According to Born stability, cubic elastic constants C_{11}, C_{12}, and C_{44} must prove the following conditions; C_{11}-C_{12}>0, C_{44}>0, C_{11}+2C_{12}>0 for structural stability, and C_{12}<B<C_{11} for cubic stability.

Poisson's ratio (υ) represents the ratio between the transverse and longitudinal strain in the elastic loading direction of the material. It also gives comprehensive knowledge about the bonding type in solids. Bulk modulus (B) implies much information about the bonding strength in materials and can be explained as the resistance of a given material to external deformations. Young's modulus (E) is described as the resistance of materials under uniaxial tension and provides the material's stiffness degree; that is, the higher the value of E, the stiffer is the material. The shear moduli G and bulk moduli B are given by equations 1 and 2 respectively (Han et al., 2008).

$$B = \frac{1}{3}(C_{11} + 2C_{12}) \quad \ldots (19)$$

$$G = \frac{1}{2}(G_V + G_R) \quad \ldots (20)$$

Where;

$$G_V = \frac{1}{5}(3C_{44} + C_{11} - C_{12}) \quad \ldots (21$$

$$G_R = 5C_{44}\ (C_{11} - C_{12})/(4C_{44} + 3(C_{11} - C_{12})) \quad \ldots (22)$$

The Young's modulus E, Poisson's ratio υ, and anisotropic coefficient A are obtained according to the equation. (3), (4), and (5) respectively (Khon, 1965; Music & Schneider, 2006).

$$E = \frac{9BG}{3B + G} \quad \ldots (23)$$

$$\upsilon = \frac{3B-2G}{2(3B+G)} \quad \ldots (24)$$

$$A = \frac{2C_{44}}{C_{11}-C_{12}} \quad \ldots (25)$$

Table 4

Bulk, Shear, Young's Modulus, Poisson Ratio, Anisotropy Ratio, Pugh's Index, and Debye Temperature

Property	Present			Other (WIEN2K CODE)
	Voigt	Reus	Voigt -Reus-Hill	(Sundareswari *et al*, 2010)
Bulk Modulus (B)	168.9938GPa	168.9938GPa	168.9938GPa	166.54GPa
Young's Modulus (E)	250.5612GPa	240.6400GPa	245.6051GPa	195.34GPa
Shear Modulus (G)	107.7014GPa	87.5678GPa	97.6346GPa	74.87GPa
Poisson Ratio (ν)	0.2561	02593	0.2577	0.27
Anisotropy Ratio (A)	-	-	0.6833	0.76
Pugh's Index (G/B)	-	-	0.577	0.45
Debye Temperature, Θ_D (K)	-	-	289.136K	281.83

Bulk modulus for Niobium Tin is 166.54 GPa. This gives a measure of how the material withstands changes in volume when compressed from all sides. The capacity of a material to resist deformation is directly proportional to its bulk modulus. Shear modulus for Niobium Tin is 74.87 GPa. This is a numerical value that measures the ability of materials to resist transverse deformation. A larger value of shear modulus indicates that the solid is highly rigid and may require greater force to be deformed.

The calculated Young's modulus of 195.34 GPa indicates the tensile elasticity of a material. That is, a measure of the ability of a material to withstand variations in length when subjected to compression or lengthwise tension. It is obtained when longitudinal

stress is divided by strain, which indicates how stiff a material is. The larger the ratio, the stiffer the material.

Pugh's ratio is a limit for the ductile and brittle behavior of materials. If G/B is 0.571 and higher, the material is brittle; otherwise, the material becomes ductile. Considering this, the results in Table 4 show that Pugh's ratio is 0.577, indicating that the material is brittle. Poisson's ratio is given by calculating the ratio of the lateral strain to that of the longitudinal strain in the direction of the stretching force. Applying Pugh's criterion, a ratio below 0.26 indicates that the material is brittle, while a ratio above 2.6 indicates that the material is ductile. It can therefore be concluded that Niobium Tin is brittle since it has a Poisson's ratio of 0.2577. When Poisson's ratio is in the range 0.25–0.5, it implies that the forces in the compound are central.

The elastic anisotropy, A, of crystals is important for engineering applications since it is correlated with the possibility of producing microcracks in materials. For a completely isotropic system, the value is 1; otherwise, values of A that are less than or greater than 1 indicate anisotropy. The calculated shear anisotropic factor for Niobium Tin is 0.6833, which indicates that the material is elastically anisotropic.

CHAPTER FIVE

SUMMARY, CONCLUSION, AND RECOMMENDATIONS

5.1 Introduction

This chapter presents a summary of the study, which was carried out using first-principles computational modelling implemented in the Quantum Espresso software based on DFT. It concludes with recommendations on the study of cubic Niobium Tin.

5.2 Summary

The main objective of this study was to determine the structural, electronic, elastic, and dynamical properties of Niobium Tin and the effect of pressure on the superconducting properties of Niobium Tin and doped Niobium Tin. In this work, first-principles DFT using Thermo_PW interfaced with the Quantum Espresso Code was used to investigate the elastic properties and the mechanical stability of cubic Niobium Tin.

The structure of the Niobium Tin unit cell was visualized. The band structure indicates that the material has no band gap, hence it is a conductor. Phonon dispersions are computed, confirming that the compound is dynamically stable. A system is considered to be dynamically stable at equilibrium if the potential energy is always increasing for any combination of displacement of atoms. The phonons should therefore have non-negative and real frequencies for stability. Niobium Tin has no negative frequencies.

Elastic behaviour of materials is a true measure of how material deformations relate to external stress. The behaviour is more important in determining how best materials can change due to intrinsic and extrinsic effects that affect the atomic orientation and structural geometry. This change is highly dependent on the chemical composition, the structure of the crystal lattice, and the deforming stress.

Under pressure, a material undergoes several elastic behavior changes due to the reduction of interatomic orbitals, which modifies the electronic orbitals and the order of bonding. If the structure remains unaffected by the loading stress, the electronic properties get highly modified. Some of these modifications include: broadening of the band gap, change of the Fermi energy, induction of a semiconductor to conductor change, and change of ordering of the electronic states. Niobium Tin is affected by pressure, but its electronic properties remain relatively unchanged.

The calculated values for elastic constants for the material were found to be in line with the Born and Hung conditions for mechanical stability. In addition, the values of the elastic constants indicated that the material studied lacked resistance against deformation.

Titanium-doped Niobium Tin's critical temperature exhibits a slight response to pressure changes, in contrast to Niobium Tin, which shows a relatively drastic response. Titanium-doped Niobium is more stable to the effects of pressure compared to Niobium Tin, as the changes in application under pressure are minimal. The Poisson ratio, anisotropy ratio, and Pugh's index show a larger change in pressure for Niobium Tin compared to dope Niobium Tin. The materials' thermal conductivity was deduced from their Debye temperature.

5.2.1 Comparison with Other Studies and Reasons for Differences

The results of this study show notable consistency with previous theoretical work on Niobium Tin in terms of its electronic properties and superconducting behaviour. Like other studies, it confirms that Niobium Tin is a metallic conductor with no band gap, and that its phonon dispersion spectrum shows dynamic stability. However, the study distinguishes itself by placing a greater emphasis on pressure-dependent elastic and mechanical behavior, particularly through the introduction of Titanium doping. While

many earlier studies focus on intrinsic superconducting properties or magnetic behavior, this research extends into how mechanical stability changes under pressure a relatively underexplored area.

The observed difference especially the minimal response of doped Niobium Tin to pressure may be attributed to the modification of lattice dynamics and bonding strength introduced by Titanium atoms, which is not extensively reported in prior work. The enhanced mechanical resilience of Titanium-doped Niobium Tin underlines the importance of targeted doping as a stabilization mechanism, offering a more application-oriented outlook than many fundamental studies, which stop at band structure or basic superconducting characteristics.

5.2.2 Implications for Research and Practical Applications

The findings from this study have significant implications for both academic research and real-world applications. From a research perspective, the clear documentation of how pressure alters elastic properties along with the comparative stability of doped materials provides a strong foundation for designing more resilient superconductors, especially for use in environments where mechanical stress is inevitable (e.g., high-field magnets in MRI machines, fusion reactors, or particle accelerators).

Practically, materials like Titanium-doped Niobium Tin, which show minimal performance variation under pressure, are highly valuable in the development of superconducting magnets or components in aerospace and energy sectors. The improved stability reduces the risk of quenching (sudden loss of superconductivity) and mechanical failure, thus improving the safety, efficiency, and longevity of superconducting systems.

5.2.3 Research Directions Based on Current Findings

Building on the current findings, several promising research directions emerge:

i. **Advanced Dopant Screening**: Explore other transition metal dopants (e.g., Vanadium, Zirconium, or Hafnium) to determine if they can further enhance mechanical and thermal stability without compromising superconducting performance. Computational screening combined with experimental validation would be an effective approach.

ii. **Anisotropy-Dependent Applications**: Since pressure affects elastic anisotropy differently in doped versus undoped materials, future research can explore **orientation-specific performance** how different crystallographic directions respond under mechanical or thermal stress. This has implications for textured or polycrystalline applications.

5.3 Conclusion

The Knowledge of superconducting properties at varying pressures, elastic constants, dynamical properties, and electronic structure properties will help engineers design and fabricate materials suitable for different applications and varying conditions. From this study, the results obtained can be used to guide experimentalists in coming up with improved Niobium Tin superconductors. Niobium Tin is a superconductor. The material is dynamically stable. From its elastic constants, the material is brittle. It is highly susceptible to changes in pressure. Titanium-doped Niobium Tin is more resistant to changes caused by deforming stress.

5.4 Recommendations

Further Suggestions for Future Research Based on Findings

Additional research avenues could include:

i. Superconducting Gap and Electron-Phonon Coupling Analysis: Investigate the changes in the superconducting gap and electron-phonon interaction parameters under pressure and doping. These are fundamental to understanding the exact mechanisms behind the observed changes in critical temperature.

ii. Pressure-Induced Phase Transitions: Explore whether extreme pressures can induce phase transitions in doped variants and how these transitions influence superconductivity or mechanical behaviour.

REFERENCES

Bagayoko, D. (2014). Understanding density functional theory (DFT) and applying it in practice. *AIP Advances*, *4*(12).

Barth, C., Seeber, B., Rack, A., Calzolaio, C., Zhai, Y., Matera, D., & Senatore, C. (2018). Quantitative correlation between the void morphology of niobium-tin wires and their irreversible critical current degradation upon mechanical loading. *Scientific Reports*, *8*(1), 6589.

Bendjemil, B., Hafs, A., Benaldjia, A., & Vrel, D. (2012). Superconducting NbTi by combustion synthesis. *International Journal of Self-Propagating High-Temperature Synthesis*, *21*, 117-123.

Bickelhaupt, F. M., & Baerends, E. J. (2000). Kohn-Sham density functional theory: predicting and understanding chemistry. *Reviews in computational chemistry*, 1-86.

Bruce, A. Z. (2005). *A High Current Density Low Cost Niobium 3 Tin Titanium Doped Conductor Utilizing A Novel Internal Tin Process* (No. INIS-US--0683). Supergenics LLC (United States). Funding organisation: USDOE Office of Science and Technology (OST)(EM-50)(United States).

Burke, K., & Wagner, L. O. (2013). DFT in a nutshell. *International Journal of Quantum Chemistry*, *113*(2), 96-101.

Cherkaev, A. V., & Gibiansky, L. V. (1993). Coupled estimates for the bulk and shear moduli of a two-dimensional isotropic elastic composite. *Journal of the Mechanics and Physics of Solids*, *41*(5), 937-980.

Chiesa, L. (2006). Development of an Experiment to study the effects of transverse stress on the critical current of a Niobium-tin superconducting cable.

Corso, A. D. (2018). SISSA, the International School for Advanced Studies, SISSA – Trieste, De Marzi, G., Bordini, B., & Baffar

Dynes, R. C., Garno, J. P., & Waszczak, J. V. (1972). Direct measurement of the superconducting energy gap in thin-film aluminum. *Physical Review Letters*, *28*(19), 1344–1347. https://doi.org/10.1103/PhysRevLett.28.1344

Ferreira, L., Rezende, S. C., Pinto da Silva, A. A. A., Poirier, G. Y., Coelho, G. C., & Ramos, A. S. (2017, August). Microstructure and Oxidation Resistance of Mechanically Alloyed and Sintered Ni-Nb and Ni-Nb-Ta Alloys. In *Materials Science Forum* (Vol. 899, pp. 19-24). Trans Tech Publications Ltd.

Freda, R., Chiarelli, S., Corato, V., della Corte, A., De Marzi, G., Di Zenobio, A., ... & Viola, R. (2014). Performance test of superconducting wires subject to heavy deformations. *IEEE Transactions on Applied Superconductivity*, *25*(3), 1-4.

G. De Marzi and L. Morici ENEA UTFUS-COND C. R. Frascatita,

Godeke, A., Den Ouden, A., Nijhuis, A., & ten Kate, H. H. (2008). State-of-the-art powder-in-tube niobium–tin superconductors. *Cryogenics*, *48*(7-8), 308-316.

Han, T., Krohn, D., Wang, L. T., & Zhu, W. (2010). New physics signals in longitudinal gauge boson scattering at the LHC. *Journal of High Energy Physics*, *2010*(3), 1-24.

Hong, S., Field, M. B., Parrell, J. A., & Zhang, Y. (2006). Latest improvements in the current carrying capability of niobium tin and its magnet applications. *IEEE transactions on applied superconductivity*, *16*(2), 1146-1151.

i, D. (2021). On the mechanisms governing the critical current reduction in Nb3Sn Rutherford cables under transverse stress. *Scientific Reports*, *11*(1), 7369.

Imai, T., Ahilan, K., Ning, F. L., McQueen, T. M., & Cava, R. J. (2009). Why does undoped FeSe become a high-Tc superconductor under pressure?. *Physical Review Letters*, *102*(17), 177005.

] E. G¨uler and M. G¨uler, Adv. Mater. Sci. Eng. 2013, Article ID 525673 (2013). [2] E. G¨uler and M. G¨uler, Mater. Res. Ibero. Am. J. 17, 1268 (2014).

Kamerlingh Onnes, H. (1911). *Further experiments with liquid helium. G. On the change of electric resistance of pure metals at very low temperatures, etc. IV. The resistance of pure mercury at helium temperatures* (Vol. 120b). Communications from the Physical Laboratory of the University of Leiden.

Kohn, W. (1999). Nobel lecture: Electronic structure of matter—Wave functions and density functionals. *Reviews of Modern Physics*, *71*(5), 1253–1266. https://doi.org/10.1103/RevModPhys.71.1253

Kohn, W., & Sham, L. J. (1965). Self-consistent equations including exchange and correlation effects. *Physical review*, *140*(4A), A1

Koretsune, T., & Arita, R. (2017). Efficient method to calculate the electron–phonon coupling constant and superconducting transition temperature. *Computer Physics Communications*, *220*, 239–242. https://doi.org/10.1016/j.cpc.2017.07.011

Loria, R., De Marzi, G., Anzellini, S., Muzzi, L., Pompeo, N., Gala, F., ... & Meneghini, C. (2016). The Effect of Hydrostatic Pressure on the Superconducting and Structural Properties of Nb $ _3 $ Sn: Ab-initio Modeling and SR-XRD Investigation. *IEEE Transactions on Applied Superconductivity*, *27*(4), 1-5.

Marzi, G., Author2, A. A., Author3, B. B., & Author4, C. C. (2005). *Title of the article in sentence case: Subtitle if available*. *Title of the Journal in Italics*, *volume number*(issue number), page range. https://doi.org/xxxxx

Mayrhofer, P. H., Music, D., & Schneider, J. M. (2006). Influence of the Al distribution on the structure, elastic properties, and phase stability of supersaturated Ti1− xAlxN. *Journal of Applied Physics*, *100*(9).

Melcher, F., Graupner, T., Gäbler, H. E., Sitnikova, M., Oberthür, T., Gerdes, A., ... & Chudy, T. (2017). Mineralogical and chemical evolution of tantalum–(niobium–tin) mineralisation in pegmatites and granites. Part 2: Worldwide examples (excluding Africa) and an overview of global metallogenetic patterns. *Ore Geology Reviews*, *89*, 946-987.

Morita, T., Yagai, T., Banno, N., & Nimori, S. (2021). Influence of Ti doping on the Nb_3 Sn layer formation for various Nb_3 Sn wire structures. *Proceedings of the 27th International Conference on Magnet Technology (MT-27)*.

Mouhat F and Coudert F X 2014 Necessary and sufficient elastic stability conditions in various crystal systems Phys. Rev. B - Condens. Matter Mater. Phys. 90 4–7

Murnaghan, F. D. (1944). The compressibility of media under extreme pressures. *Proceedings of the National Academy of Sciences of the United States of America, 30*(9), 244–247. https://doi.org/10.1073/pnas.30.9.244

Perdew JP, Chevary JA, Vosko S, et al. Atoms, molecules, solids, and surfaces: Applications of the generalized gradient approximation for exchange and correlation. Phys Rev B. 1992; 46:6671.

Poirier, R., Plamondon, R., Cheeke, J. D. N., & Bussiere, J. F. (1984). Elastic constants of polycrystalline Nb3Sn between 4.2 and 300 K. *Journal of applied physics*, *55*(9), 3327-3332.

Pugh, S. F. (1954). XCII. Relations between the elastic moduli and the plastic properties of polycrystalline pure metals. *The London, Edinburgh, and Dublin Philosophical Magazine and Journal of Science*, *45*(367), 823-843.

Ravindran, P., Fast, L., Korzhavyi, P. A., Johansson, B., Wills, J., & Eriksson, O. (1998). Density functional theory for calculation of elastic properties of orthorhombic crystals: Application to TiSi 2. *Journal of Applied Physics*, *84*(9), 4891-4904.

Rivlin, R. S., & Ericksen, J. L. (1997). Stress-deformation relations for isotropic materials. *Collected Papers of RS Rivlin: Volume I and II*, 911-1013.

Sasmal, K., Lv, B., Lorenz, B., Guloy, A. M., Chen, F., Xue, Y. Y., & Chu, C. W. (2008). Superconducting Fe-based compounds (A 1− x Sr x) Fe 2 As 2 with A= K and Cs with transition temperatures up to 37 K. *Physical Review Letters*, *101*(10), 107007.

Schleder, G. R., Padilha, A. C., Acosta, C. M., Costa, M., & Fazzio, A. (2019). From DFT to machine learning: recent approaches to materials science–a review. *Journal of Physics: Materials*, *2*(3), 032001.

Sundareswari, M., Ramasubramanian, S., & Rajagopalan, M. (2010). Elastic and thermodynamical properties of A15 Nb3X (X= Al, Ga, In, Sn and Sb) compounds—First principles DFT study. *Solid state communications*, *150*(41-42), 2057-2060

Van Delft, D., & Kes, P. (2010). The discovery of superconductivity. *Physics today*, *63*(9), 3

Wang, B., Liu, Y., Ye, J. W., & Wang, J. (2013). Electronic, magnetic and elastic properties of Mo2FeB2: first-principles calculations. *Computational materials science*, *70*, 133-139.

Wu, L.-N., Yang, S.-T., Shen, J.-K., Zhang, J.-S., & Liu, F.-H. (2023). Coexistence of superconductivity and charge density wave instability in A15-Nb_3 Sn. *Physical Chemistry Chemical Physics*, 25, 32452–32459. https://doi.org/10.10 39/D3 CP04614A

Xu, X., Sumption, M. D., & Peng, X. (2015). Internally oxidized Nb3Sn strands with fine grain size and high critical current density. *Advanced Materials*, *27*(8), 1346-1350.

Zhang, R., Gao, P., Wang, X., & Zhou, Y. (2015). First-principles study on elastic and superconducting properties of Nb_3 Sn and Nb_3 Al under hydrostatic pressure. *AIP Advances*, *5*(10), 107233. https://doi.org/10.1063/1.4935099 ADS+2

Zhang, L., & Niu, Q. (2015). Valley contrasting chiral phonons in monolayer hexagonal lattices. *arXiv*. https://arxiv.org/abs/1502.02573

Zhang, Y. (2016). First-principles Debye–Callaway approach to lattice thermal conductivity. *Journal of Materiomics*, *2*(3), 237-247.

APPENDICES

Appendix I: Input an output File for Pwscf Code

& CONTROL

calculation = 'scf'

restart_mode = 'from_scratch',

outdir = './'

prefix = 'NbSn'

pseudo_dir = './'

etot_conv_thr = 1e-5

tprnfor = .true.

/

&SYSTEM

ibrav =1,

celldm (1) =10.0071,

nat = 8,

ntyp = 2,

ecutwfc =40.0,

ecutrho = 320,

!nbnd = 64,

noncolin=.true.

lspinorb=.true.

!spin=2

degauss = 0.01,

occupations = 'smearing', smearing='gaussian', degauss=0.03

starting_magnetization = 0.5

/

&ELECTRONS

conv_thr = 1e-11

/

ATOMIC_SPECIES

Sn 118.71 Sn.pbe-dn-kjpaw_psl.1.0.0.UPF

Nb 92.9064 Nb.pbe-spn-kjpaw_psl.1.0.0.UPF

ATOMIC_POSITIONS {crystal}

```
 Nb      0.25000000000000   0.00000000000000   0.50000000000000
 Nb      0.75000000000000  -0.00000000000000   0.50000000000000
 Nb      0.50000000000000   0.25000000000000  -0.00000000000000
 Nb      0.50000000000000   0.75000000000000   0.00000000000000
 Nb     -0.00000000000000   0.50000000000000   0.25000000000000
 Nb      0.00000000000000   0.50000000000000   0.75000000000000
 Sn      0.00000000000000   0.00000000000000   0.00000000000000
 Sn      0.50000000000000   0.50000000000000   0.50000000000000
K_POINTS {automatic}
 10 10 10 0 0 0
```

Output file

```
    Program PWSCF v.5.1 starts on 11Jan2024 at 18: 6: 5
    This program is part of the open-source Quantum ESPRESSO suite
    for quantum simulation of materials; please cite
        "P. Giannozzi et al., J. Phys.:Condens. Matter 21 395502 (2009);
         URL http://www.quantum-espresso.org",
    in publications or presentations arising from this work. More details at
    http://www.quantum-espresso.org/quote
    Parallel version (MPI), running on     1 processors
    Waiting for input...
    Reading input from standard input
Warning: card / ignored

    Current dimensions of program PWSCF are:
    Max number of different atomic species (ntypx) = 10
    Max number of k-points (npk) =  40000
    Max angular momentum in pseudopotentials (lmaxx) =  3
            file Sn.pbe-dn-kjpaw_psl.1.0.0.UPF: wavefunction(s)  5S 5P 4D renormalized
            file Nb.pbe-spn-kjpaw_psl.1.0.0.UPF: wavefunction(s)  4S 4P 4D renormalized

    Subspace diagonalization in iterative solution of the eigenvalue problem:
    A serial algorithm will be used
    G-vector sticks info
    --------------------
```

sticks: dense smooth PW G-vecs: dense smooth PW
Sum 2561 1281 373 97137 34265 5449
bravais-lattice index = 1
lattice parameter (alat) = 10.0071 a.u.
unit-cell volume = 1002.1315 (a.u.)^3
number of atoms/cell = 8
number of atomic types = 2
number of electrons = 106.00
number of Kohn-Sham states= 64
kinetic-energy cutoff = 40.0000 Ry
charge density cutoff = 320.0000 Ry
convergence threshold = 1.0E-08
mixing beta = 0.3000
number of iterations used = 8 plain mixing
Exchange-correlation = SLA PW PBX PBC (1 4 3 4 0)

celldm(1)= 10.007100 celldm(2)= 0.000000 celldm(3)= 0.000000
celldm(4)= 0.000000 celldm(5)= 0.000000 celldm(6)= 0.000000

crystal axes: (cart. coord. in units of alat)
a(1) = (1.000000 0.000000 0.000000)
a(2) = (0.000000 1.000000 0.000000)
a(3) = (0.000000 0.000000 1.000000)
reciprocal axes: (cart. coord. in units 2 pi/alat)
b(1) = (1.000000 0.000000 0.000000)
b(2) = (0.000000 1.000000 0.000000)
b(3) = (0.000000 0.000000 1.000000)
PseudoPot. # 1 for Sn read from file:
./Sn.pbe-dn-kjpaw_psl.1.0.0.UPF
MD5 checksum: 67f11dec737d427557dc41ea34975807
Pseudo is Projector augmented-wave + core cor, Zval = 14.0
Generated using "atomic" code by A. Dal Corso v.6.3
Shape of augmentation charge: PSQ

Using a radial grid of 1243 points, 6 beta functions with:

l(1) = 0

l(2) = 0

l(3) = 1

l(4) = 1

l(5) = 2

l(6) = 2

Q(r) pseudized with 0 coefficients

PseudoPot. # 2 for Nb read from file:

./Nb.pbe-spn-kjpaw_psl.1.0.0.UPF

MD5 check sum: dcedcbb129af9a7271e4748e5febedb1

Pseudo is Projector augmented-wave + core cor, Zval = 13.0

Generated using "atomic" code by A. Dal Corso v.6.2.2

Shape of augmentation charge: PSQ

Using a radial grid of 1227 points, 6 beta functions with:

l(1) = 0

l(2) = 0

l(3) = 1

l(4) = 1

l(5) = 2

l(6) = 2

Q(r) pseudized with 0 coefficients

atomic species valence mass pseudopotential

Sn 14.00 118.71000 Sn (1.00)

Nb 13.00 92.90640 Nb (1.00)

48 Sym. Ops., with inversion, found (24 have fractional translation)

Cartesian axes

site n. atom positions (alat units)

1 Nb tau(1) = (0.2500000 0.0000000 0.5000000)

2 Nb tau(2) = (0.7500000 0.0000000 0.5000000)

3 Nb tau(3) = (0.5000000 0.2500000 0.0000000)

4 Nb tau(4) = (0.5000000 0.7500000 0.0000000)

5 Nb tau(5) = (0.0000000 0.5000000 0.2500000)

6 Nb tau(6) = (0.0000000 0.5000000 0.7500000)

7 Sn tau(7) = (0.0000000 0.0000000 0.0000000)

8 Sn tau(8) = (0.5000000 0.5000000 0.5000000)

number of k points= 56 gaussian smearing, width (Ry)= 0.0100

cart. coord. in units 2pi/alat

k(1) = (0.0000000 0.0000000 0.0000000), wk = 0.0020000

k(2) = (0.0000000 0.0000000 0.1000000), wk = 0.0120000

k(3) = (0.0000000 0.0000000 0.2000000), wk = 0.0120000

k(4) = (0.0000000 0.0000000 0.3000000), wk = 0.0120000

k(5) = (0.0000000 0.0000000 0.4000000), wk = 0.0120000

k(6) = (0.0000000 0.0000000 -0.5000000), wk = 0.0060000

k(7) = (0.0000000 0.1000000 0.1000000), wk = 0.0240000

k(8) = (0.0000000 0.1000000 0.2000000), wk = 0.0480000

k(9) = (0.0000000 0.1000000 0.3000000), wk = 0.0480000

k(10) = (0.0000000 0.1000000 0.4000000), wk = 0.0480000

k(11) = (0.0000000 0.1000000 -0.5000000), wk = 0.0240000

k(12) = (0.0000000 0.2000000 0.2000000), wk = 0.0240000

k(13) = (0.0000000 0.2000000 0.3000000), wk = 0.0480000

k(14) = (0.0000000 0.2000000 0.4000000), wk = 0.0480000

k(15) = (0.0000000 0.2000000 -0.5000000), wk = 0.0240000

k(16) = (0.0000000 0.3000000 0.3000000), wk = 0.0240000

k(17) = (0.0000000 0.3000000 0.4000000), wk = 0.0480000

k(18) = (0.0000000 0.3000000 -0.5000000), wk = 0.0240000

k(19) = (0.0000000 0.4000000 0.4000000), wk = 0.0240000

k(20) = (0.0000000 0.4000000 -0.5000000), wk = 0.0240000

k(21) = (0.0000000 -0.5000000 -0.5000000), wk = 0.0060000

k(22) = (0.1000000 0.1000000 0.1000000), wk = 0.0160000

k(23) = (0.1000000 0.1000000 0.2000000), wk = 0.0480000

k(24) = (0.1000000 0.1000000 0.3000000), wk = 0.0480000

k(25) = (0.1000000 0.1000000 0.4000000), wk = 0.0480000

k(26) = (0.1000000 0.1000000 -0.5000000), wk = 0.0240000

k(27) = (0.1000000 0.2000000 0.2000000), wk = 0.0480000

k(28) = (0.1000000 0.2000000 0.3000000), wk = 0.0960000
k(29) = (0.1000000 0.2000000 0.4000000), wk = 0.0960000
k(30) = (0.1000000 0.2000000 -0.5000000), wk = 0.0480000
k(31) = (0.1000000 0.3000000 0.3000000), wk = 0.0480000
k(32) = (0.1000000 0.3000000 0.4000000), wk = 0.0960000
k(33) = (0.1000000 0.3000000 -0.5000000), wk = 0.0480000
k(34) = (0.1000000 0.4000000 0.4000000), wk = 0.0480000
k(35) = (0.1000000 0.4000000 -0.5000000), wk = 0.0480000
k(36) = (0.1000000 -0.5000000 -0.5000000), wk = 0.0120000
k(37) = (0.2000000 0.2000000 0.2000000), wk = 0.0160000
k(38) = (0.2000000 0.2000000 0.3000000), wk = 0.0480000
k(39) = (0.2000000 0.2000000 0.4000000), wk = 0.0480000
k(40) = (0.2000000 0.2000000 -0.5000000), wk = 0.0240000
k(41) = (0.2000000 0.3000000 0.3000000), wk = 0.0480000
k(42) = (0.2000000 0.3000000 0.4000000), wk = 0.0960000
k(43) = (0.2000000 0.3000000 -0.5000000), wk = 0.0480000
k(44) = (0.2000000 0.4000000 0.4000000), wk = 0.0480000
k(45) = (0.2000000 0.4000000 -0.5000000), wk = 0.0480000
k(46) = (0.2000000 -0.5000000 -0.5000000), wk = 0.0120000
k(47) = (0.3000000 0.3000000 0.3000000), wk = 0.0160000
k(48) = (0.3000000 0.3000000 0.4000000), wk = 0.0480000
k(49) = (0.3000000 0.3000000 -0.5000000), wk = 0.0240000
k(50) = (0.3000000 0.4000000 0.4000000), wk = 0.0480000
k(51) = (0.3000000 0.4000000 -0.5000000), wk = 0.0480000
k(52) = (0.3000000 -0.5000000 -0.5000000), wk = 0.0120000
k(53) = (0.4000000 0.4000000 0.4000000), wk = 0.0160000
k(54) = (0.4000000 0.4000000 -0.5000000), wk = 0.0240000
k(55) = (0.4000000 -0.5000000 -0.5000000), wk = 0.0120000
k(56) = (-0.5000000 -0.5000000 -0.5000000), wk = 0.0020000
Dense grid: 97137 G-vectors FFT dimensions: (60, 60, 60)
Smooth grid: 34265 G-vectors FFT dimensions: (45, 45, 45)
Largest allocated arrays est. size (Mb) dimensions
Kohn-Sham Wavefunctions 4.24 Mb (4337, 64)
NL pseudopotentials 9.53 Mb (4337, 144)

```
   Each V/rho on FFT grid          3.30 Mb     (  216000)
   Each G-vector array             0.74 Mb     (   97137)
   G-vector shells                 0.01 Mb     (     679)
Largest temporary arrays     est. size (Mb)     dimensions
   Auxiliary wavefunctions        16.94 Mb     (    4337,  256)
   Each subspace H/S matrix        1.00 Mb     (     256,  256)
   Each <psi_i|beta_j> matrix      0.14 Mb     (     144,   64)
   Arrays for rho mixing          26.37 Mb     (  216000,    8)
Initial potential from superposition of free atoms
starting charge  105.98938, renormalised to 106.00000
Starting wfc are   96 randomized atomic wfcs
Checking if some PAW data can be deallocated.
total cpu time spent up to now is       58.9 secs
Per-process dynamical memory:   317.5 Mb
Self-consistent Calculation
Iteration #  1     ecut=    40.00 Ry     beta=0.30
Davidson diagonalization with overlap
ethr =  1.00E-02,  avg # of iterations =  2.0
Threshold (ethr) on eigenvalues was too large:
Diagonalizing with lowered threshold
Davidson diagonalization with overlap
ethr =  2.08E-04,  avg # of iterations =  2.0
total cpu time spent up to now is      252.0 secs
total energy              =   -2889.74698755 Ry
Harris-Foulkes estimate   =   -2889.83303373 Ry
estimated scf accuracy    <       0.23835882 Ry
iteration #  2     ecut=    40.00 Ry     beta=0.30
Davidson diagonalization with overlap
ethr =  2.25E-04,  avg # of iterations =  2.1
total cpu time spent up to now is      345.4 secs
total energy              =   -2889.73553941 Ry
Harris-Foulkes estimate   =   -2889.76191519 Ry
estimated scf accuracy    <       0.05980383 Ry
iteration #  3     ecut=    40.00 Ry     beta=0.30
```

Davidson diagonalization with overlap
ethr = 5.64E-05, avg # of iterations = 2.2
total cpu time spent up to now is 460.6 secs
total energy = -2889.74430271 Ry
Harris-Foulkes estimate = -2889.74471599 Ry
estimated scf accuracy < 0.00434487 Ry
iteration # 4 ecut= 40.00 Ry beta=0.30
Davidson diagonalization with overlap
ethr = 4.10E-06, avg # of iterations = 6.7
total cpu time spent up to now is 583.8 secs
total energy = -2889.74478015 Ry
Harris-Foulkes estimate = -2889.74470597 Ry
estimated scf accuracy < 0.00076003 Ry
iteration # 5 ecut= 40.00 Ry beta=0.30
Davidson diagonalization with overlap
ethr = 7.17E-07, avg # of iterations = 2.5
total cpu time spent up to now is 678.1 secs
total energy = -2889.74478486 Ry
Harris-Foulkes estimate = -2889.74481705 Ry
estimated scf accuracy < 0.00005188 Ry
iteration # 6 ecut= 40.00 Ry beta=0.30
Davidson diagonalization with overlap
ethr = 4.89E-08, avg # of iterations = 3.4
total cpu time spent up to now is 806.5 secs
total energy = -2889.74479766 Ry
Harris-Foulkes estimate = -2889.74479794 Ry
estimated scf accuracy < 0.00000403 Ry
iteration # 7 ecut= 40.00 Ry beta=0.30
Davidson diagonalization with overlap
ethr = 3.81E-09, avg # of iterations = 3.9
total cpu time spent up to now is 925.2 secs
total energy = -2889.74479846 Ry
Harris-Foulkes estimate = -2889.74479989 Ry
estimated scf accuracy < 0.00000311 Ry

iteration # 8 ecut= 40.00 Ry beta=0.30
Davidson diagonalization with overlap
ethr = 2.94E-09, avg # of iterations = 2.7
total cpu time spent up to now is 1037.1 secs
total energy = -2889.74479920 Ry
Harris-Foulkes estimate = -2889.74479907 Ry
estimated scf accuracy < 0.00000012 Ry
iteration # 9 ecut= 40.00 Ry beta=0.30
Davidson diagonalization with overlap
ethr = 1.12E-10, avg # of iterations = 4.1
total cpu time spent up to now is 1157.5 secs
total energy = -2889.74479931 Ry
Harris-Foulkes estimate = -2889.74479924 Ry
estimated scf accuracy < 0.00000001 Ry
iteration # 10 ecut= 40.00 Ry beta=0.30
Davidson diagonalization with overlap
ethr = 1.15E-11, avg # of iterations = 3.1
total cpu time spent up to now is 1294.7 secs
total energy = -2889.74479934 Ry
Harris-Foulkes estimate = -2889.74479931 Ry
estimated scf accuracy < 0.00000001 Ry
iteration # 11 ecut= 40.00 Ry beta=0.30
Davidson diagonalization with overlap
ethr = 1.15E-11, avg # of iterations = 3.1
total cpu time spent up to now is 1408.7 secs
End of self-consistent calculation
k = 0.3000 0.3000 0.4000 (4293 PWs) bands (ev):
-37.1550 -37.1397 -37.1071 -37.0363 -37.0035 -37.0002 -13.8262 -13.8074
-13.5915 -13.3923 -13.3744 -13.3295 -13.3122 -13.1758 -13.1504 -13.1250
-13.1161 -13.0784 -13.0498 -13.0285 -13.0243 -12.9934 -12.7849 -12.7782
-3.5176 -3.5165 -3.5158 -3.5139 -3.4991 -3.4981 -3.4948 -3.4932
-3.4916 -3.4906 9.3749 9.5526 13.0164 13.1845 13.6825 14.1407
14.3962 14.8870 15.3622 15.3737 15.5282 16.0775 16.1243 16.2573
16.6309 16.6717 16.9179 17.1525 17.1539 17.3399 17.7100 17.9276

18.5443 18.6689 19.5759 19.7863 19.8415 19.9559 20.0588 20.1386

k = 0.3000 0.3000-0.5000 (4280 PWs) bands (ev):

-37.1466 -37.1466 -37.0725 -37.0725 -37.0020 -37.0020 -13.8167 -13.8167
-13.4112 -13.4112 -13.3466 -13.3466 -13.2637 -13.2637 -13.1739 -13.1739
-13.1066 -13.1066 -13.0471 -13.0471 -13.0259 -13.0259 -12.7813 -12.7813
-3.5163 -3.5163 -3.5135 -3.5135 -3.4992 -3.4992 -3.4918 -3.4918
-3.4908 -3.4908 9.4994 9.4994 13.0420 13.0420 13.9408 13.9408
14.6548 14.6548 15.4426 15.4426 15.7312 15.7312 16.1680 16.1680
16.7340 16.7340 17.1227 17.1227 17.3764 17.3764 17.7767 17.7767
18.3431 18.3431 19.6337 19.6337 19.8862 19.8862 20.0145 20.0145

k = 0.3000 0.4000 0.4000 (4296 PWs) bands (ev):

-37.1467 -37.1191 -37.1028 -37.0406 -37.0313 -37.0022 -13.8175 -13.6119
-13.5809 -13.3909 -13.3827 -13.3202 -13.2831 -13.1812 -13.1654 -13.1265
-13.1247 -13.0818 -13.0581 -13.0358 -13.0315 -12.9946 -12.9915 -12.7809
-3.5171 -3.5167 -3.5153 -3.5143 -3.5003 -3.4986 -3.4964 -3.4938
-3.4931 -3.4913 9.5039 9.5982 13.0293 13.2280 13.7489 14.1841
14.3591 14.7731 15.4429 15.4690 15.5522 15.9447 16.1458 16.3320
16.6514 16.9543 17.1182 17.1973 17.2720 17.3348 17.6003 17.7257
18.2750 18.3913 19.5325 19.5598 19.8418 19.9153 19.9783 20.1489

k = 0.3000 0.4000-0.5000 (4286 PWs) bands (ev):

-37.1450 -37.1145 -37.0736 -37.0726 -37.0348 -37.0024 -13.8174 -13.5982
-13.4141 -13.3981 -13.3618 -13.3495 -13.2683 -13.2362 -13.1816 -13.1622
-13.1117 -13.1080 -13.0677 -13.0509 -13.0338 -13.0332 -12.9934 -12.7807
-3.5162 -3.5162 -3.5138 -3.5136 -3.5006 -3.4968 -3.4951 -3.4939
-3.4936 -3.4912 9.5860 9.5862 13.0089 13.2069 13.9773 14.0178
14.5074 14.5885 15.4666 15.5971 15.6318 15.6979 16.1712 16.3077
16.7074 17.0557 17.2336 17.3157 17.3674 17.4310 17.5390 17.7225
18.0351 18.1655 19.4188 19.6162 19.6993 19.8207 20.0553 20.1086

k = 0.3000-0.5000-0.5000 (4296 PWs) bands (ev):

-37.1444 -37.0882 -37.0741 -37.0741 -37.0599 -37.0026 -13.8177 -13.4155
-13.4155 -13.3685 -13.3625 -13.3504 -13.3504 -13.2210 -13.1933 -13.1592
-13.1592 -13.1160 -13.0777 -13.0777 -13.0387 -13.0356 -13.0356 -12.7804

-3.5168 -3.5168 -3.5138 -3.5138 -3.5019 -3.4973 -3.4973 -3.4952
-3.4950 -3.4917 9.6209 9.6209 12.9738 13.2574 14.1012 14.1012
14.3349 14.5384 15.5718 15.5718 15.5902 15.6617 16.1775 16.3115
16.7316 17.2959 17.2959 17.4087 17.4087 17.4145 17.6008 17.7980
17.7980 17.9088 19.2570 19.6601 19.6726 19.6726 19.9630 20.2286

k = 0.4000 0.4000 0.4000 (4269 PWs) bands (ev):

-37.1209 -37.1069 -37.1069 -37.0387 -37.0387 -37.0315 -13.6051 -13.6051
-13.5827 -13.3987 -13.3963 -13.2820 -13.2820 -13.1829 -13.1683 -13.1261
-13.1261 -13.0712 -13.0712 -13.0489 -13.0489 -12.9962 -12.9937 -12.9937
-3.5149 -3.5149 -3.5127 -3.5127 -3.4976 -3.4976 -3.4942 -3.4928
-3.4926 -3.4926 9.6083 9.6580 13.2392 13.5199 13.5199 14.1909
14.1909 14.5884 15.5738 15.6083 15.6083 16.1021 16.1021 16.2149
16.9400 16.9400 17.2052 17.2854 17.2854 17.3023 17.5288 17.5288
18.0789 18.0789 19.6820 19.7089 19.7089 19.8667 20.0037 20.2657

k = 0.4000 0.4000-0.5000 (4286 PWs) bands (ev):

-37.1121 -37.1121 -37.0736 -37.0736 -37.0361 -37.0361 -13.5981 -13.5981
-13.4082 -13.4082 -13.3630 -13.3630 -13.2464 -13.2464 -13.1540 -13.1540
-13.1090 -13.1090 -13.0667 -13.0667 -13.0531 -13.0531 -12.9954 -12.9954
-3.5163 -3.5163 -3.5133 -3.5133 -3.4980 -3.4980 -3.4969 -3.4969
-3.4941 -3.4941 9.6661 9.6661 13.3603 13.3603 13.8832 13.8832
14.3581 14.3581 15.6408 15.6408 15.8104 15.8104 16.1967 16.1967
16.9911 16.9911 17.3310 17.3310 17.3707 17.3707 17.5148 17.5148
17.8662 17.8662 19.6296

19.6296 19.8342 19.8342 20.1098 20.1098

k = 0.4000-0.5000-0.5000 (4280 PWs) bands (ev):

-37.1112 -37.0815 -37.0741 -37.0741 -37.0666 -37.0366 -13.5980 -13.4121
-13.4121 -13.3683 -13.3650 -13.3633 -13.3633 -13.2361 -13.1551 -13.1304
-13.1304 -13.1240 -13.0748 -13.0748 -13.0738 -13.0588 -13.0588 -12.9964
-3.5157 -3.5157 -3.5121 -3.5121 -3.4984 -3.4974 -3.4973 -3.4973
-3.4961 -3.4943 9.6980 9.6980 13.3890 13.5551 13.9156 13.9156
14.1073 14.2652 15.7382 15.7440 15.8172 15.8172 16.1459 16.1527

```
 16.9739  17.3088  17.3088  17.3676  17.3787  17.3787  17.5732  17.5732
 17.6141  17.6341  19.5354  19.7611  19.7611  19.8317  20.0288  20.1429
      k =-0.5000-0.5000-0.5000 (  4272 PWs)   bands (ev):
-37.0741 -37.0741 -37.0741 -37.0741 -37.0741 -37.0741 -13.4113 -13.4113
-13.3671 -13.3671 -13.3671 -13.3671 -13.3671 -13.3671 -13.1138 -13.1138
-13.1138 -13.1138 -13.1138 -13.1138 -13.0738 -13.0738 -13.0738 -13.0738
 -3.5128  -3.5128  -3.5128  -3.5128  -3.4974  -3.4974  -3.4974  -3.4974
 -3.4974  -3.4974   9.7288   9.7288  13.8456  13.8456  13.8456  13.8456
 13.8456  13.8456  15.9289  15.9289  15.9289  15.9289  15.9289  15.9289
 17.3540  17.3540  17.3540  17.3540  17.4358  17.4358  17.4358  17.4358
 17.4358  17.4358  19.7998  19.7998  19.7998  19.7998  19.7998  19.7998

 the Fermi energy is    17.3161 ev
!    total energy              =   -2889.74479937 Ry
     Harris-Foulkes estimate   =   -2889.74479934 Ry
     estimated scf accuracy    <        1.0E-10 Ry
     total all-electron energy =    -70549.237728 Ry
     The total energy is the sum of the following terms:
     one-electron contribution =    -149.42043240 Ry
     hartree contribution      =     151.78517599 Ry
     xc contribution           =    -208.08071802 Ry
     ewald contribution        =    -809.33767016 Ry
     one-center paw contrib.   =   -1874.68187310 Ry
     smearing contrib. (-TS)   =      -0.00928168 Ry
     convergence has been achieved in  11 iterations
     Writing output data file NbSn.save
     init_run     :     58.03s CPU     58.22s WALL (       1 calls)
     electrons    :   1344.22s CPU   1349.88s WALL (       1 calls)
     Called by init_run:
     wfcinit      :     51.93s CPU     52.03s WALL (       1 calls)
     potinit      :      2.53s CPU      2.56s WALL (       1 calls)
     Called by electrons:
     c_bands      :   1151.65s CPU   1157.03s WALL (      12 calls)
     sum_band     :    150.68s CPU    150.88s WALL (      12 calls)
```

v_of_rho : 1.95s CPU 1.97s WALL (12 calls)

newd : 16.79s CPU 16.83s WALL (12 calls)

mix_rho : 0.21s CPU 0.22s WALL (12 calls)

Called by c_bands:

init_us_2 : 5.71s CPU 5.88s WALL (1400 calls)

cegterg : 1132.33s CPU 1137.53s WALL (672 calls)

Called by *egterg:

h_psi : 630.61s CPU 631.27s WALL (2849 calls)

s_psi : 135.06s CPU 135.21s WALL (2849 calls)

g_psi : 2.05s CPU 1.95s WALL (2121 calls)

cdiaghg : 50.98s CPU 50.96s WALL (2737 calls)

Called by h_psi:

add_vuspsi : 135.34s CPU 135.20s WALL (2849 calls)

General routines

calbec : 191.06s CPU 191.26s WALL (3521 calls)

fft : 0.93s CPU 1.02s WALL (192 calls)

ffts : 0.03s CPU 0.05s WALL (24 calls)

fftw : 373.41s CPU 373.87s WALL (264748 calls)

interpolate : 0.20s CPU 0.20s WALL (24 calls)

Parallel routines

fftscatter : 22.05s CPU 22.24s WALL (264964 calls)

PAW routines

PAW_pot : 26.52s CPU 26.53s WALL (12 calls)

PAW_symme : 0.06s CPU 0.06s WALL (24 calls)

PWSCF : 23m23.45s CPU 23m29.69s WALL

This run was terminated on: 18:29:34 11Jan2024

Appendix II: Input and Output File for Bands

& control

calculation='bands'

restart_mode='from_scratch',

prefix='NbSn',

```
   pseudo_dir = './',
   outdir='./tempdir'

   tstress=.TRUE
   tprnfor=.TRUE
   etot_conv_thr =1e-5
   forc_conv_thr =1e-4
 /
 &system
   ibrav=1, celldm(1)=10.1493, nat= 8, ntyp=2,
   ecutwfc =35.0,
   lda_plus_u   = .FALSE.
   nbnd        = 64
   occupations='tetrahedra', smearing ="gaussian", degauss=0.01, ecutrho=320.0,
 /
 &electrons
   conv_thr =  1.0d-8
   mixing_beta = 0.5
   electron_maxstep = 200
/
!CELL_PARAMETERS {alat}
!4.8835080000 0.0000000000 0.0000000000
!0.0000000000 4.8835080000 0.0000000000
!0.0000000000 0.0000000000 4.8835080000
ATOMIC_SPECIES
Nb 92.9064 Nb.pbe-spn-kjpaw_psl.0.3.0.UPF
Sn 118.71  Sn_pbe_v1.uspp.F.UPF

ATOMIC_POSITIONS {crystal}
  Nb      0.25000000000000   0.00000000000000   0.50000000000000
  Nb      0.75000000000000  -0.00000000000000   0.50000000000000
  Nb      0.50000000000000   0.25000000000000  -0.00000000000000
  Nb      0.50000000000000   0.75000000000000   0.00000000000000
  Nb     -0.00000000000000   0.50000000000000   0.25000000000000
```

```
 Nb      0.00000000000000   0.50000000000000   0.75000000000000
 Sn      0.00000000000000   0.00000000000000   0.00000000000000
 Sn      0.50000000000000   0.50000000000000   0.50000000000000
K_POINTS (crystal_b)
 12
 0.0000   0.0000   0.0000  20 !\Gamma
 0.0000   0.5000   0.0000  20 !X
 0.0000   0.5000   0.0000  20 !X
 0.5000   0.5000   0.0000  20 !M
 0.5000   0.5000   0.0000  20 !M
 0.0000   0.0000   0.0000  20 !\Gamma
 0.0000   0.0000   0.0000  20 !\Gamma
 0.5000   0.5000   0.5000  20 !R
 0.5000   0.5000   0.5000  20 !R
 0.0000   0.5000   0.0000  20 !X
 0.5000   0.5000   0.0000  20 !M
 0.5000   0.5000   0.5000  20 !R
```

```
NbSn
&inputph
   prefix = 'NbSn'
   amass(1) = 118.71
   amass(2) = 92.9064
   outdir = './'

   tr2_ph = 1e-11

   fildvscf = 'NbSndv'
   fildyn = 'NbSn.dyn'
   alpha_mix = 0.2
   verbosity = 'high'
   ldisp = .true.
   elop = .false.
   electron_phonon = 'simple'
   el_ph_sigma = 0.02
```

```
    el_ph_nsigma = 10
    trans = .true.
    nq1 = 2, nq2 = 2, nq3 = 2

  Program PWSCF v.5.1 starts on 24Jan2024 at 14: 3:12
     This program is part of the open-source Quantum ESPRESSO suite
     for quantum simulation of materials; please cite
        "P. Giannozzi et al., J. Phys.:Condens. Matter 21 395502 (2009);
         URL http://www.quantum-espresso.org",
     in publications or presentations arising from this work. More details at
     http://www.quantum-espresso.org/quote
     Parallel version (MPI), running on     1 processors
     Waiting for input...
     Reading input from standard input
     Current dimensions of program PWSCF are:
     Max number of different atomic species (ntypx) = 10
     Max number of k-points (npk) =  40000
     Max angular momentum in pseudopotentials (lmaxx) =  3
     Atomic positions and unit cell read from directory:
     ./NbSn.save/
           file Sn.pbe-dn-kjpaw_psl.1.0.0.UPF: wavefunction(s)  5S 5P 4D renormalized
           file Nb.pbe-spn-kjpaw_psl.1.0.0.UPF: wavefunction(s)  4S 4P 4D renormalized
     Fixed quantization axis for GGA:     0.000000    0.000000    1.000000
     Message from routine setup:
     At least one non s.o. pseudo
     Subspace diagonalization in iterative solution of the eigenvalue problem:
     a serial algorithm will be used


     G-vector sticks info
     --------------------
     sticks:   dense  smooth     PW     G-vecs:    dense   smooth      PW
     Sum         2561    1281    373              97137    34265    5449
     Generating pointlists ...
     new r_m :   0.2306 (alat units)  2.3076 (a.u.) for type    1
```

new r_m :   0.2063 (alat units) 2.0640 (a.u.) for type   2

bravais-lattice index   =   1

lattice parameter (alat) =   10.0071 a.u.

unit-cell volume   =   1002.1315 (a.u.)^3

number of atoms/cell   =   8

number of atomic types   =   2

number of electrons   =   106.00

number of Kohn-Sham states=   128

kinetic-energy cutoff   =   40.0000 Ry

charge density cutoff   =   320.0000 Ry

Exchange-correlation   = SLA PW   PBX PBC (1 4 3 4 0)

Noncollinear calculation with spin-orbit

celldm(1)= 10.007100 celldm(2)=   0.000000 celldm(3)=   0.000000

celldm(4)=   0.000000 celldm(5)=   0.000000 celldm(6)=   0.000000

crystal axes: (cart. coord. in units of alat)

a(1) = (1.000000   0.000000   0.000000)

a(2) = (0.000000   1.000000   0.000000)

a(3) = (0.000000   0.000000   1.000000)

reciprocal axes: (cart. coord. in units 2 pi/alat)

b(1) = (1.000000 0.000000 0.000000)

b(2) = (0.000000 1.000000 0.000000)

b(3) = (0.000000 0.000000 1.000000)

PseudoPot. # 1 for Sn read from file:

./Sn.pbe-dn-kjpaw_psl.1.0.0.UPF

MD5 check sum: 67f11dec737d427557dc41ea34975807

Pseudo is Projector augmented-wave + core cor, Zval = 14.0

Generated using "atomic" code by A. Dal Corso v.6.3

Shape of augmentation charge: PSQ

Using radial grid of 1243 points, 6 beta functions with:

l(1) =   0

l(2) =   0

l(3) =   1

l(4) =   1

l(5) =   2

```
            l(6) =   2
    Q(r) pseudized with 0 coefficients
    PseudoPot. # 2 for Nb read from file:
    ./Nb.pbe-spn-kjpaw_psl.1.0.0.UPF
    MD5 check sum: dcedcbb129af9a7271e4748e5febedb1
    Pseudo is Projector augmented-wave + core cor, Zval = 13.0
    Generated using "atomic" code by A. Dal Corso  v.6.2.2
    Shape of augmentation charge: PSQ
    Using radial grid of 1227 points,  6 beta functions with:
            l(1) =   0
            l(2) =   0
            l(3) =   1
            l(4) =   1
            l(5) =   2
            l(6) =   2
    Q(r) pseudized with 0 coefficients
    atomic species   valence    mass     pseudopotential
      Sn             14.00   118.71000     Sn( 1.00)
      Nb             13.00    92.90640     Nb( 1.00)
    16 Sym. Ops., with inversion, found (24 have fractional translation)
                               s                 frac. trans.
     isym =  1     identity
Time Reversal           0
cryst.   s( 1) = (     1         0         0      )
                 (     0         1         0      )
                 (     0         0         1      )
cart.    s( 1) = (  1.0000000  0.0000000  0.0000000 )
                 (  0.0000000  1.0000000  0.0000000 )
                 (  0.0000000  0.0000000  1.0000000 )
     isym =  2     180 deg rotation - cart. axis [0,0,1]

Time Reversal           0
cryst.   s( 2) = (    -1         0         0      )
                 (     0        -1         0      )
```

```
                ( 0 0 1 )
cart. s( 2) = ( -1.0000000 0.0000000 0.0000000 )
                ( 0.0000000 -1.0000000 0.0000000 )
                ( 0.0000000 0.0000000 1.0000000 )
    isym = 3 180 deg rotation - cart. axis [0,1,0]

Time Reversal 1
cryst. s( 3) = ( -1 0 0 )
                ( 0 1 0 )
                ( 0 0 -1 )
cart. s( 3) = ( -1.0000000 0.0000000 0.0000000 )
                ( 0.0000000 1.0000000 0.0000000 )
                ( 0.0000000 0.0000000 -1.0000000 )
    isym = 4 180 deg rotation - cart. axis [1,0,0]
Time Reversal 1
cryst. s( 4) = ( 1 0 0 )
                ( 0 -1 0 )
                ( 0 0 -1 )
cart. s( 4) = ( 1.0000000 0.0000000 0.0000000 )
                ( 0.0000000 -1.0000000 0.0000000 )
                ( 0.0000000 0.0000000 -1.0000000 )
    isym = 5 180 deg rotation - cart. axis [1,1,0]
Time Reversal 1
cryst. s( 5) = ( 0 1 0 ) f =( -0.5000000 )
                ( 1 0 0 ) ( -0.5000000 )
                ( 0 0 -1 ) ( 0.5000000 )
cart. s( 5) = ( 0.0000000 1.0000000 0.0000000 ) f =( -0.5000000 )
                ( 1.0000000 0.0000000 0.0000000 ) ( -0.5000000 )
                ( 0.0000000 0.0000000 -1.0000000 ) ( 0.5000000 )
   isym = 6 180 deg rotation - cart. axis [1,-1,0]

Time Reversal 1
cryst. s( 6) = ( 0 -1 0 ) f =( 0.5000000 )
                ( -1 0 0 ) ( 0.5000000 )
```

```
                ( 0 0 -1 ) ( 0.5000000 )

cart. s( 6) = ( 0.0000000 -1.0000000 0.0000000 ) f =( 0.5000000 )
                ( -1.0000000 0.0000000 0.0000000 ) ( 0.5000000 )
                ( 0.0000000 0.0000000 -1.0000000 ) ( 0.5000000 )
    isym = 7 90 deg rotation - cart. axis [0,0,-1]
Time Reversal 0
cryst. s( 7) = ( 0 -1 0 ) f =( -0.5000000 )
                ( 1 0 0 ) ( 0.5000000 )
                ( 0 0 1 ) ( 0.5000000 )
cart. s( 7) = ( 0.0000000 1.0000000 0.0000000 ) f =( -0.5000000 )
                ( -1.0000000 0.0000000 0.0000000 ) ( 0.5000000 )
                ( 0.0000000 0.0000000 1.0000000 ) ( 0.5000000 )
    isym = 8 90 deg rotation - cart. axis [0,0,1]

Time Reversal 0
cryst. s( 8) = ( 0 1 0 ) f =( 0.5000000 )
                ( -1 0 0 ) ( -0.5000000 )
                ( 0 0 1 ) ( 0.5000000 )
cart. s( 8) = ( 0.0000000 -1.0000000 0.0000000 ) f =( 0.5000000 )
                ( 1.0000000 0.0000000 0.0000000 ) ( -0.5000000 )
                ( 0.0000000 0.0000000 1.0000000 ) ( 0.5000000 )


    isym = 9 inversion
Time Reversal 0
cryst. s( 9) = ( -1 0 0 )
                ( 0 -1 0 )
                ( 0 0 -1 )
cart. s( 9) = ( -1.0000000 0.0000000 0.0000000 )
                ( 0.0000000 -1.0000000 0.0000000 )
                ( 0.0000000 0.0000000 -1.0000000 )
    isym = 10 inv. 180 deg rotation - cart. axis [0,0,1]
```

Time Reversal 0

cryst. s(10) = (1 0 0)

(0 1 0)

(0 0 -1)

cart. s(10) = (1.0000000 0.0000000 0.0000000)

(0.0000000 1.0000000 0.0000000)

(0.0000000 0.0000000 -1.0000000)

isym = 11 inv. 180 deg rotation - cart. axis [0,1,0]

Time Reversal 1

cryst. s(11) = (1 0 0)

(0 -1 0)

(0 0 1)

cart. s(11) = (1.0000000 0.0000000 0.0000000)

(0.0000000 -1.0000000 0.0000000)

(0.0000000 0.0000000 1.0000000)

isym = 12 inv. 180 deg rotation - cart. axis [1,0,0]

Time Reversal 1

cryst. s(12) = (-1 0 0)

(0 1 0)

(0 0 1)

cart. s(12) = (-1.0000000 0.0000000 0.0000000)

(0.0000000 1.0000000 0.0000000)

(0.0000000 0.0000000 1.0000000)

isym = 13 inv. 180 deg rotation - cart. axis [1,1,0]

Time Reversal 1

cryst. s(13) = (0 -1 0) f =(0.5000000)

(-1 0 0) (0.5000000)

(0 0 1) (0.5000000)

cart. s(13) = (0.0000000 -1.0000000 0.0000000) f =(0.5000000)

(-1.0000000 0.0000000 0.0000000) (0.5000000)

(0.0000000 0.0000000 1.0000000) (0.5000000)

isym = 14 inv. 180 deg rotation - cart. axis [1,-1,0]

Time Reversal 1

cryst. s(14) = (0 1 0) f =(-0.5000000)
(1 0 0) (-0.5000000)
(0 0 1) (0.5000000)

cart. s(14) = (0.0000000 1.0000000 0.0000000) f =(-0.5000000)
(1.0000000 0.0000000 0.0000000) (-0.5000000)
(0.0000000 0.0000000 1.0000000) (0.5000000)

isym = 15 inv. 90 deg rotation - cart. axis [0,0,-1]

Time Reversal 0

cryst. s(15) = (0 1 0) f =(0.5000000)
(-1 0 0) (-0.5000000)
(0 0 -1) (0.5000000)

cart. s(15) = (0.0000000 -1.0000000 0.0000000) f =(0.5000000)
(1.0000000 0.0000000 0.0000000) (-0.5000000)
(0.0000000 0.0000000 -1.0000000) (0.5000000)

isym = 16 inv. 90 deg rotation - cart. axis [0,0,1]

Time Reversal 0

cryst. s(16) = (0 -1 0) f =(-0.5000000)
(1 0 0) (0.5000000)
(0 0 -1) (0.5000000)

cart. s(16) = (0.0000000 1.0000000 0.0000000) f =(-0.5000000)
(-1.0000000 0.0000000 0.0000000) (0.5000000)
(0.0000000 0.0000000 -1.0000000) (0.5000000)

the magnetic double point group is D_4h(4/mmm) [C_4h (4/m)]

using the double point group C_4h (4/m)

there are 16 classes and 8 irreducible representations

the character table:

	E	-E	C4	-C4	C4^2	-C4^2	C4^3	-C4^3	i	-i	S4^3	-S4^3
G_5+	1.00	-1.00	0.71	-0.71	0.00	0.00	0.71	-0.71	1.00	-1.00	0.71	-0.71
G_6+	1.00	-1.00	0.71	-0.71	0.00	0.00	0.71	-0.71	1.00	-1.00	0.71	-0.71
G_7+	1.00	-1.00	-0.71	0.71	0.00	0.00	-0.71	0.71	1.00	-1.00	-0.71	0.71
G_8+	1.00	-1.00	-0.71	0.71	0.00	0.00	-0.71	0.71	1.00	-1.00	-0.71	0.71

G_5-	1.00	-1.00	0.71	-0.71	0.00	0.00	0.71	-0.71	-1.00	1.00	-0.71	0.71
G_6-	1.00	-1.00	0.71	-0.71	0.00	0.00	0.71	-0.71	-1.00	1.00	-0.71	0.71
G_7-	1.00	-1.00	-0.71	0.71	0.00	0.00	-0.71	0.71	-1.00	1.00	0.71	-0.71
G_8-	1.00	-1.00	-0.71	0.71	0.00	0.00	-0.71	0.71	-1.00	1.00	0.71	-0.71

	E	-E	C4	-C4	C4^2	-C4^2	C4^3	-C4^3	i	-i	S4^3	-S4^3
G_5+	0.00	0.00	0.71	-0.71	1.00	-1.00	-0.71	0.71	0.00	0.00	0.71	-0.71
G_6+	0.00	0.00	-0.71	0.71	-1.00	1.00	0.71	-0.71	0.00	0.00	-0.71	0.71
G_7+	0.00	0.00	-0.71	0.71	1.00	-1.00	0.71	-0.71	0.00	0.00	-0.71	0.71
G_8+	0.00	0.00	0.71	-0.71	-1.00	1.00	-0.71	0.71	0.00	0.00	0.71	-0.71
G_5-	0.00	0.00	0.71	-0.71	1.00	-1.00	-0.71	0.71	0.00	0.00	-0.71	0.71
G_6-	0.00	0.00	-0.71	0.71	-1.00	1.00	0.71	-0.71	0.00	0.00	0.71	-0.71
G_7-	0.00	0.00	-0.71	0.71	1.00	-1.00	0.71	-0.71	0.00	0.00	0.71	-0.71
G_8-	0.00	0.00	0.71	-0.71	-1.00	1.00	-0.71	0.71	0.00	0.00	-0.71	0.71

	s_h	-s_h	S4	-S4
G_5+	1.00	-1.00	-0.71	0.71
G_6+	-1.00	1.00	0.71	-0.71
G_7+	1.00	-1.00	0.71	-0.71
G_8+	-1.00	1.00	-0.71	0.71
G_5-	-1.00	1.00	0.71	-0.71
G_6-	1.00	-1.00	-0.71	0.71
G_7-	-1.00	1.00	-0.71	0.71
G_8-	1.00	-1.00	0.71	-0.71

Cartesian axes

site n.	atom	positions (alat units)
1	Nb	tau(1) = (0.2500000 0.0000000 0.5000000)
2	Nb	tau(2) = (0.7500000 0.0000000 0.5000000)
3	Nb	tau(3) = (0.5000000 0.2500000 0.0000000)
4	Nb	tau(4) = (0.5000000 0.7500000 0.0000000)
5	Nb	tau(5) = (0.0000000 0.5000000 0.2500000)
6	Nb	tau(6) = (0.0000000 0.5000000 0.7500000)
7	Sn	tau(7) = (0.0000000 0.0000000 0.0000000)
8	Sn	tau(8) = (0.5000000 0.5000000 0.5000000)

Crystallographic axes

site n. atom positions (cryst. coord.)

1 Nb tau(1) = (0.2500000 0.0000000 0.5000000)

2 Nb tau(2) = (0.7500000 0.0000000 0.5000000)

3 Nb tau(3) = (0.5000000 0.2500000 0.0000000)

4 Nb tau(4) = (0.5000000 0.7500000 0.0000000)

5 Nb tau(5) = (0.0000000 0.5000000 0.2500000)

6 Nb tau(6) = (0.0000000 0.5000000 0.7500000)

7 Sn tau(7) = (0.0000000 0.0000000 0.0000000)

8 Sn tau(8) = (0.5000000 0.5000000 0.5000000)

number of k points= 221 gaussian smearing, width (Ry)= 0.0300

cart. coord. in units 2pi/alat

k(1) = (0.0000000 0.0000000 0.0000000), wk = 0.0000000

k(2) = (0.0000000 0.0250000 0.0000000), wk = 0.0000599

k(21) = (0.0000000 0.5000000 0.0000000), wk = 0.0011980

k(22) = (0.0000000 0.5000000 0.0000000), wk = 0.0011980

k(23) = (0.0000000 0.5000000 0.0000000), wk = 0.0011980

k(24) = (0.0000000 0.5000000 0.0000000), wk = 0.0011980

k(25) = (0.0000000 0.5000000 0.0000000), wk = 0.0011980

k(26) = (0.0000000 0.5000000 0.0000000), wk = 0.0011980

k(27) = (0.0000000 0.5000000 0.0000000), wk = 0.0011980

k(28) = (0.0000000 0.5000000 0.0000000), wk = 0.0011980

k(29) = (0.0000000 0.5000000 0.0000000), wk = 0.0011980

k(30) = (0.0000000 0.5000000 0.0000000), wk = 0.0011980

k(31) = (0.0000000 0.5000000 0.0000000), wk = 0.0011980

k(32) = (0.0000000 0.5000000 0.0000000), wk = 0.0011980

k(33) = (0.0000000 0.5000000 0.0000000), wk = 0.0011980

k(34) = (0.0000000 0.5000000 0.0000000), wk = 0.0011980

k(35) = (0.0000000 0.5000000 0.0000000), wk = 0.0011980

k(36) = (0.0000000 0.5000000 0.0000000), wk = 0.0011980

k(37) = (0.0000000 0.5000000 0.0000000), wk = 0.0011980

k(38) = (0.0000000 0.5000000 0.0000000), wk = 0.0011980

k(39) = (0.0000000 0.5000000 0.0000000), wk = 0.0011980

k(40) = (0.0000000 0.5000000 0.0000000), wk = 0.0011980

k(41) = (0.0000000 0.5000000 0.0000000), wk = 0.0011980

k(42) = (0.0250000 0.5000000 0.0000000), wk = 0.0012579

k(43) = (0.0500000 0.5000000 0.0000000), wk = 0.0013178

k(44) = (0.0750000 0.5000000 0.0000000), wk = 0.0013777

k(45) = (0.1000000 0.5000000 0.0000000), wk = 0.0014376

k(46) = (0.1250000 0.5000000 0.0000000), wk = 0.0014975

k(47) = (0.1500000 0.5000000 0.0000000), wk = 0.0015574

k(48) = (0.1750000 0.5000000 0.0000000), wk = 0.0016173

k(49) = (0.2000000 0.5000000 0.0000000), wk = 0.0016772

k(50) = (0.2250000 0.5000000 0.0000000), wk = 0.0017371

k(51) = (0.2500000 0.5000000 0.0000000), wk = 0.0017970

k(52) = (0.2750000 0.5000000 0.0000000), wk = 0.0018569

k(53) = (0.3000000 0.5000000 0.0000000), wk = 0.0019168

k(54) = (0.3250000 0.5000000 0.0000000), wk = 0.0019767

00000 0.0000000), wk = 0.0040902

k(113) = (0.0000000 0.0000000 0.0000000), wk = 0.0040902

k(114) = (0.0000000 0.0000000 0.0000000), wk = 0.0040902

k(115) = (0.0000000 0.0000000 0.0000000), wk = 0.0040902

k(116) = (0.0000000 0.0000000 0.0000000), wk = 0.0040902

k(117) = (0.0000000 0.0000000 0.0000000), wk = 0.0040902

k(118) = (0.0000000 0.0000000 0.0000000), wk = 0.0040902

k(119) = (0.0000000 0.0000000 0.0000000), wk = 0.0040902

k(120) = (0.0000000 0.0000000 0.0000000), wk = 0.0040902

k(121) = (0.0000000 0.0000000 0.0000000), wk = 0.0040902

k(122) = (0.0250000 0.0250000 0.0250000), wk = 0.0041940

k(123) = (0.0500000 0.0500000 0.0500000), wk = 0.0042977

k(124) = (0.0750000 0.0750000 0.0750000), wk = 0.0044015

k(125) = (0.1000000 0.1000000 0.1000000), wk = 0.0045052

k(126) = (0.1250000 0.1250000 0.1250000), wk = 0.0046090

k(127) = (0.1500000 0.1500000 0.1500000), wk = 0.0047127

k(128) = (0.1750000 0.1750000 0.1750000), wk = 0.0048165

k(129) = (0.2000000 0.2000000 0.2000000), wk = 0.0049202

k(130) = (0.2250000 0.2250000 0.2250000), wk = 0.0050240

k(131) = (0.2500000 0.2500000 0.2500000), wk = 0.0051277
k(132) = (0.2750000 0.2750000 0.2750000), wk = 0.0052315
k(133) = (0.3000000 0.3000000 0.3000000), wk = 0.0053352
k(134) = (0.3250000 0.3250000 0.3250000), wk = 0.0054390
k(135) = (0.3500000 0.3500000 0.3500000), wk = 0.0055427
k(136) = (0.3750000 0.3750000 0.3750000), wk = 0.0056465
k(137) = (0.4000000 0.4000000 0.4000000), wk = 0.0057502
k(138) = (0.4250000 0.4250000 0.4250000), wk = 0.0058540
k(139) = (0.4500000 0.4500000 0.4500000), wk = 0.0059577
k(140) = (0.4750000 0.4750000 0.4750000), wk = 0.0060615

-37.0901 -37.0901 -37.0677 -37.0677 -37.0621 -37.0621 -37.0621 -37.0621
-37.0564 -37.0564 -37.0338 -37.0338 -13.5213 -13.5213 -13.4047 -13.4047
-13.4047 -13.4047 -13.3535 -13.3535 -13.3497 -13.3497 -13.3497 -13.3497
-13.3489 -13.3489 -13.2419 -13.2419 -13.1337 -13.1337 -13.1166 -13.1166
-13.1145 -13.1145 -13.1145 -13.1145 -13.0744 -13.0744 -13.0673 -13.0673
-13.0673 -13.0673 -13.0570 -13.0570 -13.0570 -13.0570 -13.0262 -13.0262
-3.5143 -3.5143 -3.5143 -3.5143 -3.5114 -3.5114 -3.5114 -3.5114
-3.4974 -3.4974 -3.4974 -3.4974 -3.4972 -3.4972 -3.4966 -3.4966
-3.4954 -3.4954 -3.4943 -3.4943 9.7107 9.7107 9.7107 9.7107
13.5002 13.5002 13.6289 13.6289 13.8844 13.8844 13.8844 13.8844
14.0435 14.0435 14.1686 14.1686 15.7821 15.7821 15.7897 15.7897
15.8675 15.8675 15.8675 15.8675 16.0980 16.0980 16.1004 16.1004
17.1097 17.1097 17.3281 17.3281 17.3281 17.3281 17.3781 17.3781
17.3781 17.3781 17.3833 17.3833 17.5320 17.5320 17.5320 17.5320
17.5685 17.5685 17.6213 17.6213 19.6099 19.6099 19.7845 19.7845
19.7845 19.7845 19.8092 19.8092 19.9834 19.9834 20.0293 20.0293

k = 0.5000 0.5000 0.4500 (4264 PWs) bands (ev):

-37.0808 -37.0808 -37.0658 -37.0658 -37.0621 -37.0621 -37.0621 -37.0621
-37.0583 -37.0583 -37.0431 -37.0431 -13.4626 -13.4626 -13.4047 -13.4047
-13.4047 -13.4047 -13.3528 -13.3528 -13.3506 -13.3506 -13.3506 -13.3506
-13.3497 -13.3497 -13.2668 -13.2668 -13.1238 -13.1238 -13.1154 -13.1154
-13.1091 -13.1091 -13.1091 -13.1091 -13.0840 -13.0840 -13.0670 -13.0670

-13.0670 -13.0670 -13.0635 -13.0635 -13.0619 -13.0619 -13.0619 -13.0619
-3.5120 -3.5120 -3.5120 -3.5120 -3.5117 -3.5117 -3.5117 -3.5117
-3.4976 -3.4976 -3.4976 -3.4976 -3.4973 -3.4973 -3.4970 -3.4970
-3.4960 -3.4960 -3.4955 -3.4955 9.7205 9.7205 9.7205 9.7205
13.6147 13.6147 13.7021 13.7021 13.8623 13.8623 13.8623 13.8623
13.9792 13.9792 14.0654 14.0654 15.8281 15.8281 15.8344 15.8344
15.9028 15.9028 15.9028 15.9028 16.0427 16.0427 16.0437 16.0437
17.2323 17.2323 17.3419 17.3419 17.3419 17.3419 17.3701 17.3701
17.3701 17.3701 17.3974 17.3974 17.4894 17.4894 17.4894 17.4894
17.5203 17.5203 17.5839 17.5839 19.6766 19.6766 19.7892 19.7892
19.7966 19.7966 19.7966 19.7966 19.9274 19.9274 19.9280 19.9280

k = 0.5000 0.5000 0.4750 (4272 PWs) bands (ev):

-37.0715 -37.0715 -37.0639 -37.0639 -37.0621 -37.0621 -37.0621 -37.0621
-37.0602 -37.0602 -37.0526 -37.0526 -13.4053 -13.4053 -13.4047 -13.4047
-13.4047 -13.4047 -13.3521 -13.3521 -13.3511 -13.3511 -13.3511 -13.3511
-13.3505 -13.3505 -13.3039 -13.3039 -13.1138 -13.1138 -13.1117 -13.1117
-13.1053 -13.1053 -13.1053 -13.1053 -13.0939 -13.0939 -13.0889 -13.0889
-13.0669 -13.0669 -13.0669 -13.0669 -13.0655 -13.0655 -13.0655 -13.0655
-3.5123 -3.5123 -3.5123 -3.5123 -3.5122 -3.5122 -3.5122 -3.5122
-3.4983 -3.4983 -3.4978 -3.4978 -3.4977 -3.4977 -3.4977 -3.4977
-3.4975 -3.4975 -3.4972 -3.4972 9.7264 9.7264 9.7264 9.7264
13.7298 13.7298 13.7740 13.7740 13.8488 13.8488 13.8488 13.8488
13.9128 13.9128 13.9567 13.9567 15.8789 15.8789 15.8820 15.8820
15.9251 15.9251 15.9251 15.9251 15.9864 15.9864 15.9881 15.9881
17.3462 17.3462 17.3556 17.3556 17.3556 17.3556 17.3644 17.3644
17.3644 17.3644 17.4181 17.4181 17.4581 17.4581 17.4581 17.4581
17.4794 17.4794 17.5253 17.5253 19.7421 19.7421 19.7860 19.7860
19.8037 19.8037 19.8037 19.8037 19.8530 19.8530 19.8680 19.8680

k = 0.5000 0.5000 0.5000 (4272 PWs) bands (ev):

-37.0621 -37.0621 -37.0621 -37.0621 -37.0621 -37.0621 -37.0621 -37.0621
-37.0620 -37.0620 -37.0620 -37.0620 -13.4047 -13.4047 -13.4047 -13.4047

-13.3513 -13.3513 -13.3513 -13.3513 -13.3513 -13.3513 -13.3513 -13.3513
-13.3513 -13.3513 -13.3513 -13.3513 -13.1038 -13.1038 -13.1038 -13.1038
-13.1038 -13.1038 -13.1038 -13.1038 -13.1038 -13.1038 -13.1038 -13.1038
-13.0668 -13.0668 -13.0668 -13.0668 -13.0668 -13.0668 -13.0668 -13.0668
-3.5122 -3.5122 -3.5122 -3.5122 -3.5122 -3.5122 -3.5122 -3.5122
-3.4978 -3.4978 -3.4978 -3.4978 -3.4978 -3.4978 -3.4978 -3.4978
-3.4978 -3.4978 -3.4978 -3.4978 9.7284 9.7284 9.7284 9.7284
13.8443 13.8443 13.8443 13.8443 13.8443 13.8443 13.8443 13.8443
13.8443 13.8443 13.8443 13.8443 15.9327 15.9327 15.9327 15.9327
15.9327 15.9327 15.9327 15.9327 15.9327 15.9327 15.9327 15.9327
17.3623 17.3623 17.3623 17.3623 17.3623 17.3623 17.3623 17.3623
17.4453 17.4453 17.4453 17.4453 17.4453 17.4453 17.4453 17.4453
17.4454 17.4454 17.4454 17.4454 19.8060 19.8060 19.8060 19.8060
19.8060 19.8060 19.8060 19.8060 19.8060 19.8060 19.8060 19.8060
13.6147 13.6147 13.7021 13.7021 13.8623 13.8623 13.8623 13.8623
13.9792 13.9792 14.0654 14.0654 15.8281 15.8281 15.8344 15.8344
15.9028 15.9028 15.9028 15.9028 16.0427 16.0427 16.0437 16.0437
17.2323 17.2323 17.3419 17.3419 17.3419 17.3419 17.3701 17.3701
17.3701 17.3701 17.3974 17.3974 17.4894 17.4894 17.4894 17.4894
17.5203 17.5203 17.5839 17.5839 19.6766 19.6766 19.7892 19.7892
19.7966 19.7966 19.7966 19.7966 19.9274 19.9274 19.9280 19.9280

k = 0.5000 0.5000 0.4750 (4272 PWs) bands (ev):

-37.0715 -37.0715 -37.0639 -37.0639 -37.0621 -37.0621 -37.0621 -37.0621
-37.0602 -37.0602 -37.0526 -37.0526 -13.4053 -13.4053 -13.4047 -13.4047
-13.4047 -13.4047 -13.3521 -13.3521 -13.3511 -13.3511 -13.3511 -13.3511
-13.3505 -13.3505 -13.3039 -13.3039 -13.1138 -13.1138 -13.1117 -13.1117
-13.1053 -13.1053 -13.1053 -13.1053 -13.0939 -13.0939 -13.0889 -13.0889
-13.0669 -13.0669 -13.0669 -13.0669 -13.0655 -13.0655 -13.0655 -13.0655
-3.5123 -3.5123 -3.5123 -3.5123 -3.5122 -3.5122 -3.5122 -3.5122
-3.4983 -3.4983 -3.4978 -3.4978 -3.4977 -3.4977 -3.4977 -3.4977
-3.4975 -3.4975 -3.4972 -3.4972 9.7264 9.7264 9.7264 9.7264
13.7298 13.7298 13.7740 13.7740 13.8488 13.8488 13.8488 13.8488
13.9128 13.9128 13.9567 13.9567 15.8789 15.8789 15.8820 15.8820
15.9251 15.9251 15.9251 15.9251 15.9864 15.9864 15.9881 15.9881

17.3462 17.3462 17.3556 17.3556 17.3556 17.3556 17.3644 17.3644
17.3644 17.3644 17.4181 17.4181 17.4581 17.4581 17.4581 17.4581
17.4794 17.4794 17.5253 17.5253 19.7421 19.7421 19.7860 19.7860
19.8037 19.8037 19.8037 19.8037 19.8530 19.8530 19.8680 19.8680

k = 0.5000 0.5000 0.5000 (4272 PWs) bands (ev):

-37.0621 -37.0621 -37.0621 -37.0621 -37.0621 -37.0621 -37.0621 -37.0621
-37.0620 -37.0620 -37.0620 -37.0620 -13.4047 -13.4047 -13.4047 -13.4047
-13.3513 -13.3513 -13.3513 -13.3513 -13.3513 -13.3513 -13.3513 -13.3513
-13.3513 -13.3513 -13.3513 -13.3513 -13.1038 -13.1038 -13.1038 -13.1038
-13.1038 -13.1038 -13.1038 -13.1038 -13.1038 -13.1038 -13.1038 -13.1038
-13.0668 -13.0668 -13.0668 -13.0668 -13.0668 -13.0668 -13.0668 -13.0668
-3.5122 -3.5122 -3.5122 -3.5122 -3.5122 -3.5122 -3.5122 -3.5122
-3.4978 -3.4978 -3.4978 -3.4978 -3.4978 -3.4978 -3.4978 -3.4978
-3.4978 -3.4978 -3.4978 -3.4978 9.7284 9.7284 9.7284 9.7284
13.8443 13.8443 13.8443 13.8443 13.8443 13.8443 13.8443 13.8443
13.8443 13.8443 13.8443 13.8443 15.9327 15.9327 15.9327 15.9327
15.9327 15.9327 15.9327 15.9327 15.9327 15.9327 15.9327 15.9327
17.3623 17.3623 17.3623 17.3623 17.3623 17.3623 17.3623 17.3623
17.4453 17.4453 17.4453 17.4453 17.4453 17.4453 17.4453 17.4453
17.4454 17.4454 17.4454 17.4454 19.8060 19.8060 19.8060 19.8060
19.8060 19.8060 19.8060 19.8060 19.8060 19.8060 19.8060 19.8060

Writing output data file NbSn.save

init_run : 12.35s CPU 12.66s WALL (1 calls)

electrons : 25114.74s CPU 25146.59s WALL (1 calls)

Called by init_run:

wfcinit : 0.00s CPU 0.00s WALL (1 calls)

potinit : 7.64s CPU 7.88s WALL (1 calls)

Called by electrons:

c_bands : 25114.72s CPU 25146.51s WALL (1 calls)

v_of_rho : 0.45s CPU 0.47s WALL (1 calls)

v_h : 0.01s CPU 0.01s WALL (1 calls)

v_xc : 0.44s CPU 0.46s WALL (1 calls)

newd : 2.33s CPU 2.34s WALL (1 calls)

```
    Called by c_bands:
    init_us_2    :      0.88s CPU      0.95s WALL (     221 calls)
    cegterg      :  24076.68s CPU  24105.22s WALL (     547 calls)

    Called by sum_band:
    Called by *egterg:
    h_psi        :   7074.80s CPU   7086.26s WALL (   10065 calls)
    s_psi        :   1434.47s CPU   1434.58s WALL (   10065 calls)
    g_psi        :     29.98s CPU     29.82s WALL (    9297 calls)
    cdiaghg      :   2255.02s CPU   2255.49s WALL (    9518 calls)
    cegterg:over :   5857.83s CPU   5858.17s WALL (    9297 calls)
    cegterg:upda :   4153.51s CPU   4153.98s WALL (    9297 calls)
    cegterg:last :   3514.74s CPU   3515.02s WALL (    1467 calls)
    Called by h_psi:
    h_psi:vloc   :   4169.78s CPU   4180.21s WALL (   10065 calls)
    h_psi:vnl    :   2881.46s CPU   2881.89s WALL (   10065 calls)
    add_vuspsi   :   1429.12s CPU   1429.32s WALL (   10065 calls)
    General routines
    calbec       :   1452.26s CPU   1452.54s WALL (   10065 calls)
    fft          :      0.12s CPU      0.19s WALL (      31 calls)
    ffts         :      0.02s CPU      0.01s WALL (       4 calls)
    fftw         :   3402.43s CPU   3410.58s WALL ( 2375596 calls)
    interpolate  :      0.03s CPU      0.03s WALL (       4 calls)
    davcio       :      1.95s CPU     52.23s WALL (     221 calls)
    Parallel routines
    fft_scatter  :    212.50s CPU    213.08s WALL ( 2375631 calls)
    PAW routines
    PAW_pot      :      7.11s CPU      7.21s WALL (       1 calls)
    PWSCF        :     6h58m CPU        7h 3m WALL

   This run was terminated on:  21: 6:46  24Jan2024
=------------------------------------------------------------------------------=
   JOB DONE.
=------------------------------------------------------------------------------=
```

Appendix III : KUREC Clearance Letter

KABARAK UNIVERSITY
OFFICE OF THE DIRECTOR
INSTITUTE OF POSTGRADUATE STUDIES

Private Bag - 20157
KABARAK, KENYA

Tel : 0773 265 999
E-mail: directorpostgraduate@kabarak.ac.ke

16th May, 2024

The Chairman,
Institutional Scientific and Ethics Revie Committee (ISERC)
Kabarak University

Dear Sir/Madam,

RE: REQUEST FOR ISERC CLEARANCE TO FACILITATE NACOSTI RESEARCH PERMIT APPLICATION

I am writing to formally request ISERC clearance for **Nyandika Abigael Nyangarisa (GMP/M/0679/05/22)**, currently enrolled in the Master's program in Physics at Kabarak University. She is conducting research entitled ***"Ab initio Computational Study of Electronic Structure and Effect of Applied Pressure on Superconducting Properties of Nb_3Sn and $Ti_xNb_{3-x}Sn$."***

The student has successfully defended her research proposal and has been granted permission to proceed with field research. Kindly provide ISERC clearance to facilitate the application for the necessary NACOSTI research permit.

Thank You.

KABARAK UNIVERSITY DIRECTOR POST GRADUATE STUDIES 1 MAY 2024 PRIVATE BAG 20157, KABARAK

Dr. Nehemiah Kiplagat, PhD
Director, Institute of Postgraduate Studies

Kabarak University Moral Code
As members of Kabarak University family, we purpose at all times and in all places, to set apart in one's heart, Jesus as Lord. (1 Peter 3:15)

Kabarak University is ISO 9001:2015 Certified

Appendix IV: NACOSTI Research Permit

REPUBLIC OF KENYA

NATIONAL COMMISSION FOR SCIENCE,TECHNOLOGY & INNOVATION

Ref No: 699519

Date of Issue: 12/August/2024

RESEARCH LICENSE

This is to Certify that Miss. ABIGAEL NYANGARISA NYANDIKA of Kabarak University, has been licensed to conduct research as per the provision of the Science, Technology and Innovation Act, 2013 (Rev.2014) in Nakuru on the topic: Ab initio computational study of electronic structure and the effect of applied pressure on superconducting properties of niobium tin and titanium doped niobium tin for the period ending : 12/August/2025.

License No: NACOSTI/P/24/38626

699519

Applicant Identification Number

Director General
NATIONAL COMMISSION FOR SCIENCE,TECHNOLOGY & INNOVATION

Verification QR Code

NOTE: This is a computer generated License. To verify the authenticity of this document, Scan the QR Code using QR scanner application.

See overleaf for conditions

Appendix V: Evidence of Conference Participation

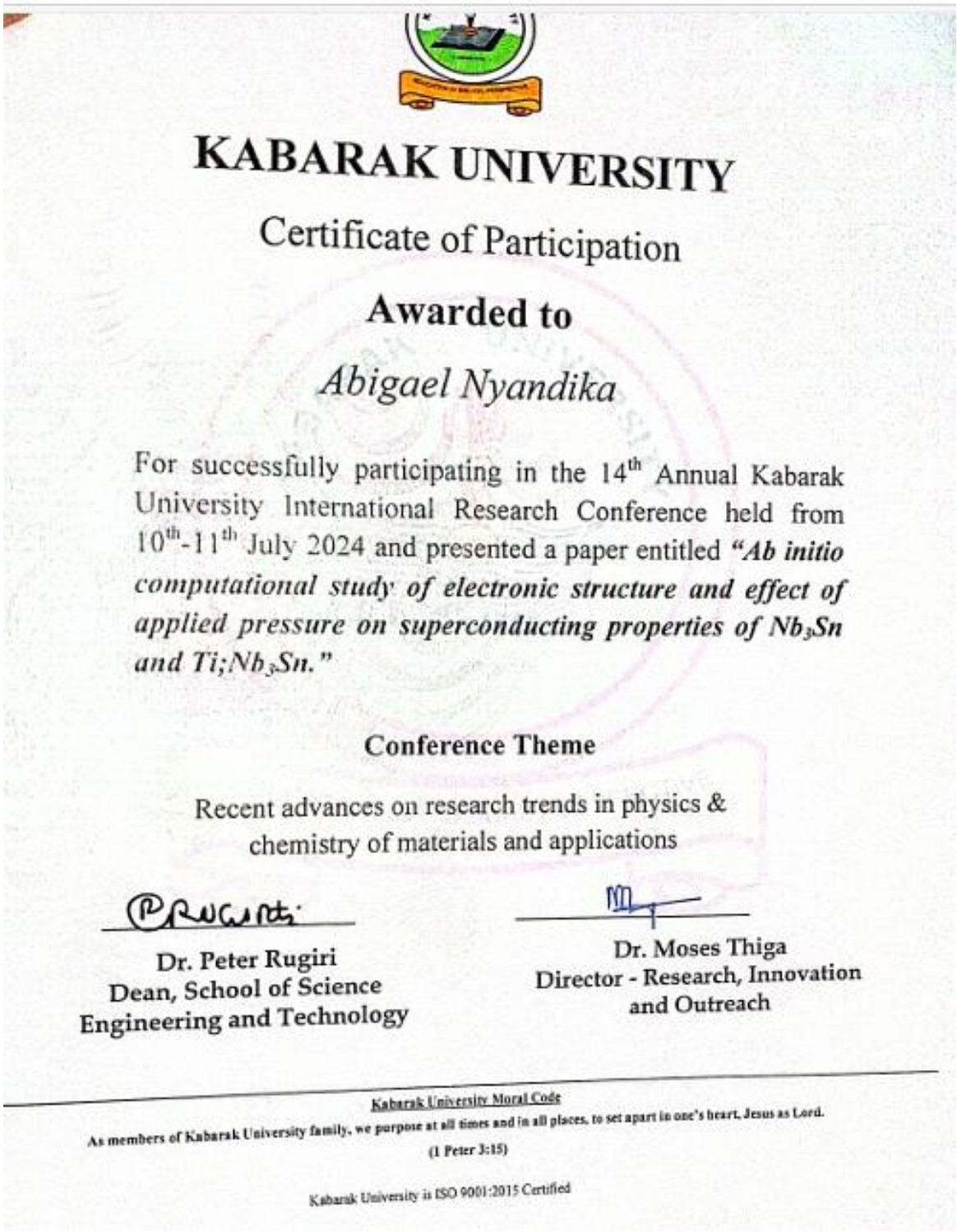

KABARAK UNIVERSITY

Certificate of Participation

Awarded to

Abigael Nyandika

For successfully participating in the 14th Annual Kabarak University International Research Conference held from 10th-11th July 2024 and presented a paper entitled ***"Ab initio computational study of electronic structure and effect of applied pressure on superconducting properties of Nb_3Sn and $Ti;Nb_3Sn$."***

Conference Theme

Recent advances on research trends in physics & chemistry of materials and applications

Dr. Peter Rugiri
Dean, School of Science Engineering and Technology

Dr. Moses Thiga
Director - Research, Innovation and Outreach

Kabarak University Moral Code

As members of Kabarak University family, we purpose at all times and in all places, to set apart in one's heart, Jesus as Lord.

(1 Peter 3:15)

Kabarak University is ISO 9001:2015 Certified

Appendix VI: List of Publication

First Principles Study of the Elastic Properties and Phonon Dispersion of Niobium Tin

Abigael NYANGARISA NYANDIKA[1], Phillip OTIENO NYAWERE[1] and Kebenei J. SELLA[1]

[1]Department of Physical and Biological Sciences, Kabarak University, P.O. Box Private Bag – 20157 Kabarak, Nakuru, Kenya.

Corresponding Author: anyandika@kabarak.ac.ke

Subimitted 4th October 2024, Accepted 18th November 2024, and Published Online 18th February 2025

ABSTRACT

The paper reports the Elastic and dynamical properties of Niobium Tin. The calculations were performed with the generalized gradient approximation functional of density functional theory with the Perdew–Burke–Ernzerhof exchange–correlation energy through virtual crystal approximation.The mechanical and dynamical properties were investigated using first principles density functional theory within the generalized gradient approximations using Quantum Espresso code which is an open source code and pseudopotentials were extracted from QE database.The code QUANTUM ESPRESSSO which is open source was used with its pseudopotential database. The elastic constants, bulk moduli, Young's moduli and shear moduli, Poisson ratio, Pugh's ratio and anisotropic ratio were also evaluated. The study on the elastic constants was done at zero pressure and it clearly indicated that the compound is stable mechanically and the phonon dispersion study also indicated that the compound is stable dynamically. The elastic constants also led to the conclusion that Niobium Tin is brittle.

Key Words: Dynamical properties, Elastic properties, Density Functional Theory

INTRODUCTION